# Supramolecular [60]fullerene chemistry on surfaces†

**Davide Bonifazi,*[ab] Olivier Enger[c] and François Diederich*[d]**

***Received 14th September 2006***
***First published as an Advance Article on the web 19th December 2006***
**DOI: 10.1039/b604308a**

This *critical review* documents the exceptional range of research avenues in [60]fullerene-based monolayers showing unique and spectacular physicochemical properties which prompted such materials to have potential applications in several directions, ranging from sensors and photovoltaic cells to nanostructured devices for advanced electronic applications, that have been pursued during the past decade. It illustrates how progress in covalent [60]fullerene functionalisation led to the development of spectacular surface-immobilised architectures, including dyads and triads for photoinduced electron and energy transfer, self-assembled on a wide variety of surfaces. All of these molecular assemblies and supramolecular arrays feature distinct properties as a consequence of the presence of different molecular units and their spatial arrangement. Since the properties of [60]fullerene-containing films are profoundly controlled by the deposition conditions, substrate of adsorption, and influenced by impurities or disordered surface structures, the progress of such new [60]fullerene-based materials strongly relies on the development of new versatile and broad preparative methodologies. Therefore, the systematic exploration of the most common approaches to prepare and characterise [60]fullerene-containing monolayers embedded into two- or three-dimensional networks will be reviewed in great detail together with their main limitations. Recent investigations hinting at potential technological applications addressing many important fundamental issues, such as a better understanding of interfacial electron transfer, ion transport in thin films, photovoltaic devices and the dynamics associated with monolayer self-assembly, are also highlighted.

[a]*Dipartimento di Scienze Farmaceutiche and INSTM UdR Trieste, Università degli Studi di Trieste, 34127 Trieste, Italy. E-mail: dbonifazi@units.it*
[b]*Département de Chimie, Facultés Universitaires Notre Dame de la Paix, B-5000 Namur, Belgium. E-mail: davide.bonifazi@fundp.ac.be*
[c]*BASF Aktiengesellschaft, GVP/C - A030, D-67056, Ludwigshafen, Germany. E-mail: olivier.enger@basf.com*
[d]*Laboratorium für Organische Chemie, ETH-Hönggerberg, CH-8093 Zürich, Switzerland. E-mail: diederich@org.chem.ethz.ch*
† The HTML version of this article has been enhanced with colour images.

## 1 Introduction

Tailored organic materials are extremely promising for applications in advanced nanoconstructed devices such as sensors, catalysts, random access memories, rechargeable power sources, solar cells, to name a few. Changing the properties of bulk materials by surface coating with structurally organised molecules has attracted considerable attention in recent years. Specifically, well-ordered monolayered or

**Davide Bonifazi**

*Davide Bonifazi was born in Guastalla (Italy) in 1975. After obtaining the "Laurea" from the University of Parma (1994–1999), and working with Prof. Enrico Dalcanale, he joined the group of Prof. François Diederich at the Swiss Federal Institute of Technology, Zürich (2000–2004). He was awarded the Silver Medallion of the ETH for his doctoral dissertation (2005). After a postdoctoral fellowship with Prof. Maurizio Prato at the University of Trieste (2004–2005), he joined the Department of Pharmaceutical Science at that university. In September 2006 he joined the Department of Chemistry at the "Facultés Universitaires Notre-Dame de la Paix" in Namur, Belgium, as junior professor. His research interests focus on the self-assembly of electronically and optically active molecules, porphyrin chemistry and functionalisation of carbon nanostructures.*

**Olivier Enger**

*Olivier Enger was born in Strasbourg, France, in 1975. He received his Master degree in Chemistry from the Université Louis Pasteur in Strasbourg in 1998. Then, he moved to the Swiss Federal Institute of Technology, Zürich, Switzerland, where he investigated the preparation, properties, and applications of [60]fullerene-based thin films under the supervision of Professor François Diederich, obtaining a PhD degree for this work in 2002. After a postdoctoral fellowship with Professor J. Fraser Stoddart at the University of California at Los Angeles, USA, studying supramolecular polymers and molecular machines, he joined BASF Aktiengesellschaft, Germany, in 2003. His research interests are on organic materials for electronic and optical applications including liquid crystals, dyes and highly conjugated materials.*

 

thin films are of great interest because of the valuable insights they provide regarding molecule interactions and their potential application to important technologies related to coatings and surface modifications. In this context, monomolecular organic layers containing functional molecules offer the possibility of transferring the molecular (electrochemical, optical or chemical) properties, as studied in solution, to a solid or liquid surface.[1] In this respect, one of the main challenges that scientists in general and chemists in particular are faced with is the production of novel chemical systems supporting real-life device properties.

Since $C_{60}$ became available in macroscopic quantities in 1990,[2] the physical properties of hollow carbon cages have been intensively investigated. Among the most spectacular physical and chemical properties, $C_{60}$ was found to behave as a strongly electron-accepting molecule able to reversibly accept up to six electrons, to show exceptional electronic absorption bands expanding throughout the entire UV-Vis spectrum, to display a strong singlet oxygen sensitising ability and to feature interesting non-linear optical properties.[3–5] However, pristine fullerenes aggregate very easily becoming insoluble or only sparingly soluble in many common organic solvents. This serious obstacle for practical applications has been overcome with the help of organic modifications of $C_{60}$. Effectively, the recent developments in the functionalisation of [60]fullerenes allow the preparation of highly soluble $C_{60}$ derivatives easier to handle.[6,7] The electronic properties, such as facile multiple reducibility, optical non-linearity or efficient photosensitisation, that are characteristic of the parent $C_{60}$ sphere are maintained for many of the fullerene derivatives.[4,8] Surface modification utilising $C_{60}$ and its covalent derivatives is currently of substantial interest, owing to the possibility of transferring the unique [60]fullerene properties to bulk materials by surface coating. Monolayers, containing redox centers at a fixed distance from a surface instead of freely diffusing, form an important class of new hybrid materials offering potential technological applications ranging from bioactive materials to advanced nanostructured devices for electronic applications. This article provides a general overview on the various approaches towards the immobilisation of $C_{60}$ and fullerene derivatives on surfaces. The physical properties of [60]fullerene-containing films are controlled by the deposition conditions and influenced by impurities or disordered surface structures. Despite extensive efforts to form stable and well-ordered [60]fullerene-containing films, the strong van der Waals interactions between the carbon spheres and the resulting tendency to form aggregates still remain one of the major issues in the formation of stable and structurally ordered films at the air–solid and air–water interface. Therefore, an absolutely essential requirement for the control and systematic exploration of the physical properties of the carbon allotropes is the development of new methodologies for the incorporation of [60]fullerene into well-defined two- and three-dimensional networks. The main methods to prepare [60]fullerene-containing monolayers or thin films are monolayer self-assembly on solid surface, Langmuir and Langmuir–Blodgett deposition techniques.

Langmuir films are prepared by spreading amphiphilic molecules on liquids surfaces, in particular water. The molecules arrange in such a way that the polar head groups have direct contact with water while the hydrophobic tails (*i.e.*, the fullerene cage) stick out into the air.[9,10] Transferring the Langmuir films onto a solid substrate (usually glass) results in the formation of Langmuir–Blodgett (LB) films which can be monolayered or multilayered depending on the number of times the substrate is dipped into the solution.[9,10] Typically, amphiphilic fullerene compounds with a hydrophilic head group that interacts with or immerses into the aqueous subphase and a hydrophobic tail are employed for the production of LB films. In view of the vast number of recent reviews summarising the research on [60]fullerene-based thin films prepared with Langmuir and Langmuir–Blodgett,[11,12] the present review will focus on the immobilisation of fullerenes on surfaces *via* the self-assembly monolayer (SAM) methodology. The different self-assembly approaches towards the construction of fullerene monolayers will be described along with all the potential applications that are currently holding great promises in materials sciences. A general overview on the preparation of SAMs and their characterisation will be shortly given in the following two Sections.

**François Diederich**

*Born in the Grand-Duchy of Luxemburg (1952), François Diederich studied chemistry at the University of Heidelberg (1971–1977). He joined the group of Prof. Heinz A. Staab for his diploma and doctoral theses which he completed in 1979 with the synthesis of kekulene. Following postdoctoral studies with Prof. Orville L. Chapman at UCLA (1979–1981), investigating arynes in Argon matrices, he returned to Heidelberg for his Habilitation at the Max-Planck-Institut für Medizinische Forschung (1981–1985). Subsequently, he joined the faculty in the Department of Chemistry and Biochemistry at UCLA where he became Full Professor of Organic and Bioorganic Chemistry in 1989. In 1992, he returned to Europe, joining the Department of Chemistry and Applied Biosciences at the ETH Zürich. His research interests, documented in more than 500 publications, are in the field of supramolecular chemistry, spanning from dendritic mimics of globular proteins, to molecular recognition studies including structure-based drug design, and to fullerene and acetylenic networks.*

### 1.1 An introduction to self-assembled monolayers (SAMs)

Self-assembled monolayers are highly ordered molecular assemblies that form spontaneously by chemisorption of functionalised molecules on surfaces, and organise themselves laterally, mostly by intermolecular van der Waals interactions.[9,13] The assembling molecules consist of three units: a head group which strongly binds to the substrate, a tail group that constitutes the outer surface of the film, and a spacer that connects head and tail and strongly affects the intermolecular separation, molecular orientation and the degree of order in

the film. The principal driving force for the formation of these films is a specific interaction between the head group and the substrate surface. Provided this interaction is strong, SAMs form robust and stable films. Depending on the structure of the molecular adsorbate, these films can be disordered or well-packed. The degree of order is a product of many factors, including geometric aspects as well as electrostatic, charge-transfer and dipole–dipole interactions within the monolayer.[9,13] The most widely studied systems are SAMs formed by chemisorption of alkanethiols on gold,[14] silver[15] or copper[16] surfaces. SAMs of phosphonates have served to synthesise multilayer structures for use in nonlinear optical devices.[17] SAMs of siloxane on glass and metallic oxides find technological use in surface treatments.[18] Although SAMs that are covalently bonded to these substrates provide rugged systems for various applications, a number of these systems—especially those based on $-SiCl_3$ or $-Si(OEt)_3$ head groups—are difficult to synthesise and the reactivity of these head groups is often incompatible with other functional groups in the molecule. SAMs are commonly prepared following three main experimental protocols: *a*) by immersion of a solid substrate into a dilute solution containing the molecule suitable for adsorption, *b*) by organic molecular beam epitaxy (OMBE) or *c*) by sublimation or evaporation in ultrahigh vacuum (UHV). The choice of the growth method strictly depends on the substrate and stability of the molecules. SAMs are particularly attractive in a great diversity of fields for several reasons: ease of preparation, tunability of surface properties through selective modification of molecular structure and function, use as a base structure for the engineering of more complex architectures, possibility of lateral structuring in the nanometer regime and high stability under ambient conditions.

### 1.2 Characterisation techniques

The total amount of organic material in a well-packed monomolecular film of fullerene molecules is on the order of $10^{-10}$ mol $cm^{-2}$. Such a small quantity of material severely limits the comprehensive characterisation by means of a single analytical technique that is capable of giving a complete structural and chemical description of a fullerene monolayer. Therefore, it is essential to use a variety of characterisation techniques in order to ascertain the most important properties of the layer, *e.g.* thickness, chemical composition, packing density and order. Only the combined information of different measurements eventually leads to an accurate picture of the thin film at the molecular and macroscopic level. The most frequently employed techniques for the characterisation of fullerene-based monolayers, and in general all monolayers, are listed in Table 1.

Wettability measurements are a simple and effective method to obtain a first impression of the structure and chemical composition of the monolayer. Contact angles of a fullerene-based monolayer with solvents such as water or hexadecane provide information about the polarity of the outer surface of the SAM, as well as the packing of the monolayer.

Infrared spectroscopy is a powerful tool for the characterisation of SAMs. The measurements of thin films on solid substrates, *e.g.* on Au, Ag and glass, are usually performed using the grazing angle reflection mode, where the incoming light is reflected under a large angle of incidence ($>80^\circ$ relative to the surface normal) to maximise the absorbance by the monolayer. Besides the usual structural data, the spectra also provide information about the average orientation of the adsorbates.

Ellipsometry is the most common optical technique to estimate the thickness of thin organic films. The operative principle is based on a plane-polarised laser beam that is reflected by the substrate, which results in a change of the phase ($\Delta$) and the amplitude ($\Psi$) of the light. Usually comparison of these two parameters for an uncovered and a covered substrate allows calculation of the thickness and the refractive index of the film. However, if the film has a thickness of less than 1/10th of the wavelength of the incident light, the changes in $\Psi$ are too small and a value for the refractive index is needed. Despite the large number of literature reports in the field of [60]fullerene-based thin films, only a few report ellipsometric data with calculated refractive index values ranging from 1.5 to 2.2 for various thick films of pristine $C_{60}$.

Atomic force microscopy (AFM) and scanning tunneling microscopy (STM) are techniques that allow the

**Table 1** Analytical techniques for SAM characterisation

| Analytical technique[a] | | Ref. | Structural information |
|---|---|---|---|
| *General* | Contact angle | 9 | Hydrophobicity and monolayer order |
| | QCM/SAW | 9,19 | Changes in mass upon self-assembly |
| *Optical* | IR spectroscopy | 20 | Nature of functional groups and molecular orientation |
| | UV-Vis absorbance | 21 | Monolayer Density |
| | Fluorescence spectroscopy | 22 | Monolayer Density |
| | Ellipsometry | 23 | Layer thickness |
| | SPR | 24 | Layer thickness |
| *Vacuum* | XPS | 21 | Elemental composition |
| | AES | 25 | Elemental composition |
| | SIMS | 26 | Molecular mass of adsorbate |
| *Microscopy* | AFM | 27 | Molecular packing |
| | STM | | Molecular packing |
| *Electrochemical* | Cyclic voltammetry | 28 | Adsorbate layer thickness, order/defects, surface coverage, |
| | Impedance spectroscopy | | Adsorbate layer thickness, order/defects |

[a] AFM: Atomic Force Microscopy; AES: Auger Electron Spectroscopy; QCM: Quartz Crystal Microbalance; SAW: Surface Acoustic Waves; SIMS: Secondary Ion Mass Spectrometry; SPR: Surface Plasmon Resonance; STM: Scanning Tunneling Microscopy; XPS: X-ray Photoelectron Spectroscopy.

 

characterisation of the packing of the adsorbates in the layer with molecular resolution *via* direct imaging.

Self-assembled monolayers bearing [60]fullerene moieties are electrochemically active monomolecular films which are mostly characterised *via* electrochemistry. Reversible electrochemistry of redox-active molecules in solution is governed by the Nernst equation, which correlates the concentration of the reduced and oxidised form of the redox-active compound at the electrode with any applied potential. In the case of a surface-confined process, cyclic voltammetry (CV) can provide valuable information about the environment of the redox centres (structure and dynamics of the monolayer). Assuming that the process starts from a surface excess of oxidised species $\Gamma_{Ox}$ (in mol cm$^{-2}$) on an electrode of area $A$ (cm$^2$), and that the redox couple Ox + $n$ e$^-$ ⇆ Red has a formal potential $E^{0'}$ and proceeds towards more negative values, in absence of any perturbation, the current maximum arises at $E = E^{0'}$ its value is given by eqn (1):

$$i_p = \frac{n^2F^2A\Gamma^*_{Ox}v}{4RT} \quad (1)$$

The direct proportionality between peak current and scan rate is a convenient test for reversible, surface-confined voltammetric behaviour. Note that while the peak current varies linearly with the scan rate, the charge under the current-potential curve does not, as it is determined by the coverage $Q$ (usually in μC cm$^{-2}$) of the excess of electroactive species, according to eqn (2):

$$Q = nFA\Gamma^*_{Ox} \quad (2)$$

In theory, the cathodic and anodic peak potentials should coincide with the formal potential value of the redox couple as the electrochemical process is not diffusion limited, and thus the whole monolayer is electrochemically addressed in one oxidation or reduction scan. In practice, however, electrodes derivatised with a fullerene layer typically exhibit a finite peak–peak splitting ($\Delta E_p$) between the two peak potentials which is usually caused by resistance effects or interactions between neighbouring fullerene cages.

## 2 Monomolecular pristine $C_{60}$-based films prepared *via* thermal evaporation or solution casting

In the crystalline form, $C_{60}$ molecules occupy the sites of a face-centered cubic (fcc) lattice with a large rotational disorder. The optical and electronic properties of solid films and crystals of pure $C_{60}$, which are insulators (bandgap *ca.* 2 eV), have been studied with increasing interest, particularly since the discovery of their superconductivity after doping with alkali metals.[29] The quality of molecular thin films strongly depends on the interactions between the molecules and between the substrates employed for their growth. Since fullerenes display much stronger intermolecular interactions and higher stability than most other organic molecules, their utilisation for molecular thin films has been vigorously investigated. Indeed, ultrahigh vacuum (UHV) deposition techniques or spin casting methods have been applied to make fullerene-containing molecular thin films, and their structure and quality have been determined by a wide range of analytical methods (*e.g.* STM, X-ray diffraction, Raman spectroscopy). Since the first report on thermal evaporation of $C_{60}$ on Au,[30] many researchers have studied the chemisorption of $C_{60}$ on a wide variety of substrates such as Au(110), Ag(111), GaAs(110), Si(111), Cu(111), mica, KBr(001) or $MoS_2$(0001).[31] The character and strength of the interaction between $C_{60}$ and the substrate essentially determine the morphology of the film growth.[32,33] In the case of strong interactions, which have been regarded as chemisorption, the mobility of the adsorbed molecules is limited and deposition leads to well-defined polycrystalline monolayers. For example, when $C_{60}$ is adsorbed onto Au(111) and Ag(111) in ultrahigh vacuum, it forms ordered films with fullerene–surface interactions of 50–60 kcal mol$^{-1}$.[32] The strong interaction with these substrates—and metallic surfaces in general—results from charge transfer from the metal into the LUMO of $C_{60}$ as demonstrated by luminescence studies.[32] For both mentioned substrates, STM studies showed that [60]fullerene molecules adopt a $2\sqrt{3} \times 2\sqrt{3}$R30° film structure, together with an additional 38 × 38 "in-phase structure" on Au(111). In contrast, for substrates, such as KBr(001), GaSe(0001), CaF(111), Si(111), freshly cleaved mica and GaAs(111), sufficiently strong van der Waals interactions between the fullerene molecules subdue the interactions between the substrate and individual $C_{60}$ molecules. This, in turn, leads to a high effective surface mobility of the physisorbed molecules and to a crystalline film growth characterised by fairly large aggregates. Besides very unusual properties, such as conductivity and superconductivity, thin solid films of $C_{60}$ and $C_{70}$, as prepared by thermal evaporation, exhibit strong optical nonlinearities.[34] As a consequence of the presence of 60 carbon atoms with 60 delocalised π-electrons, large third-order nonlinear optical responses have been reported for thin films of $C_{60}$.[35]

## 3 Preparation of [60]fullerene-based SAMs

### 3.1 Engineering approaches

Four main approaches have successfully been employed in the self-assembly of $C_{60}$ and its derivatives on surfaces (Fig. 1): *i*) functionalisation of $C_{60}$ with suitable groups that undergo a chemisorption on the surface; *ii*) pre-modification of the surface by adsorption of an organic monolayer bearing a terminal functionality that undergoes a bond-forming reaction with pristine $C_{60}$; *iii–iv*) pre-adsorbtion on the surface of an organic layer which assembles with pristine $C_{60}$ (*iii*) or its derivatives (*iv*) through non-covalent molecular recognition. While strategy *ii* often leads to defect-containing monomolecular films due to multiple additions to $C_{60}$, and *iii–iv* to films in which the [60]fullerene derivatives are only weakly bound to the surface, strategy *i* usually provides more stable and chemically homogeneous materials.

**3.1.1 Strategy i.** To our knowledge, the first example of a fullerene derivative involved in self-assembled monolayer formation was reported by Mirkin and co-workers in 1994. They first showed that fulleropyrrolidine-derived thiol **1** spontaneously adsorbs onto a Au(111)/mica substrate (Fig. 2a).[36] This led to the formation of a highly organised

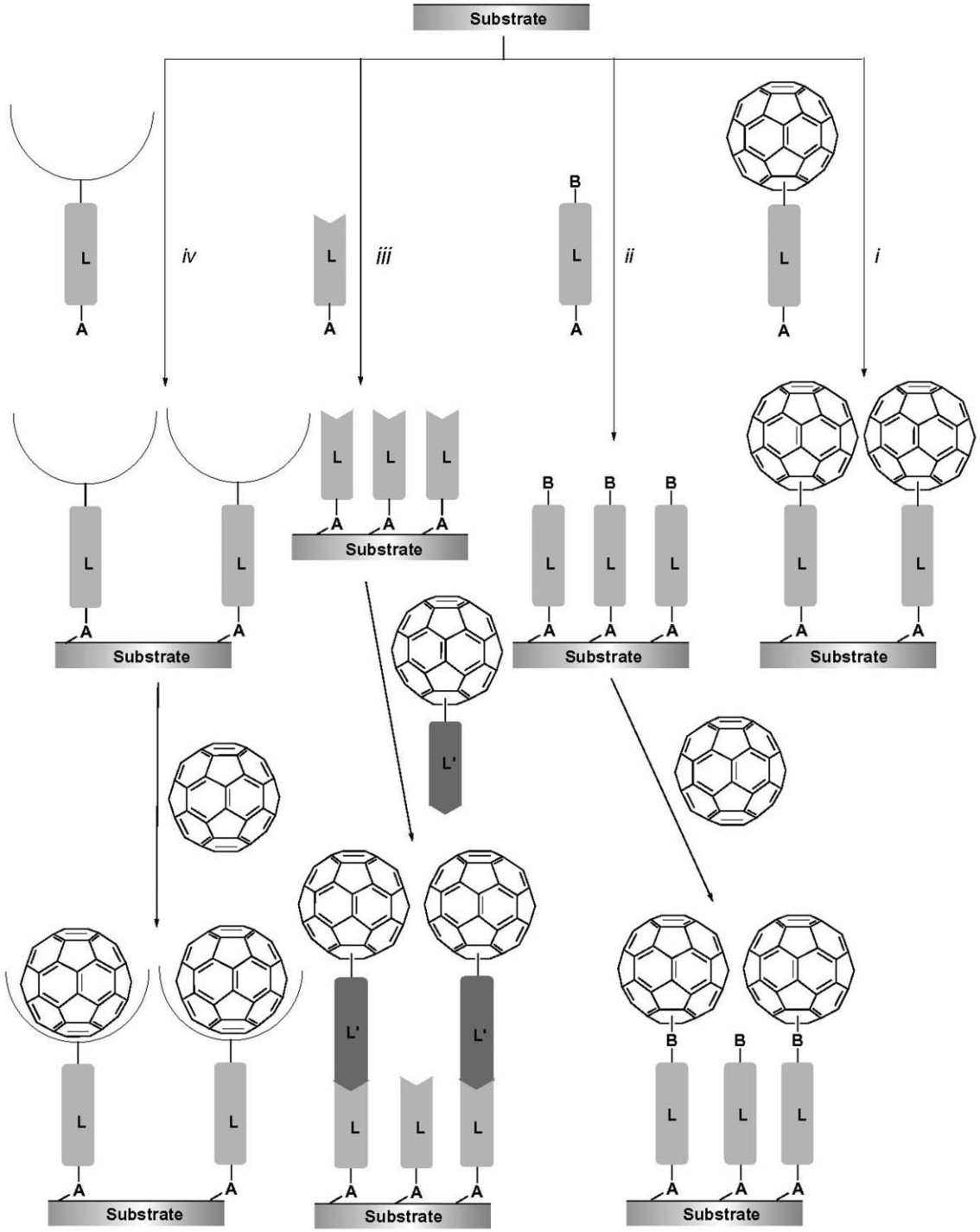


**Fig. 1** The four strategies employed to prepare fullerene-containing SAMs (**L**, **L**′ = linker; **A** = surface-binding group; **B** = group with reactivity toward $C_{60}$).

monolayer ([**1**·Au(111)]) in which the molecules are regularly spaced in a distorted hexagonal arrangement. Due to the high [60]fullerene–[60]fullerene cohesive energy ($E_{cohesive}$) of $\sim$31 kcal mol$^{-1}$,[37] the [60]fullerene cage governs the molecular packing within the monolayer ($E_{cohesive}$ is $\sim$14 kcal mol$^{-1}$ and $\sim$23 kcal mol$^{-1}$ for octane- and decanethiol,[38] respectively). The nearest [60]fullerene–[60]fullerene distance was measured as 1.09 $\pm$ 0.08 nm, which is in good agreement with the $C_{60}\cdots C_{60}$ distance (1.07 $\pm$ 0.13 nm) in a (111) face of crystalline buckminster[60]fullerene as determined by AFM measurements.[39] Cyclic voltammetric measurements of the [**1**·Au(111)] assembly revealed a full surface coverage, a cathodic shift ($E_{1/2}^{red,1}$ = $-$1.03 V and $-$1.21 V for free **1** and [**1**·Au(111)], respectively) of the first [60]fullerene-centred reduction and a linear dependence between the peak current and the scan rate. The latter two observations are

 

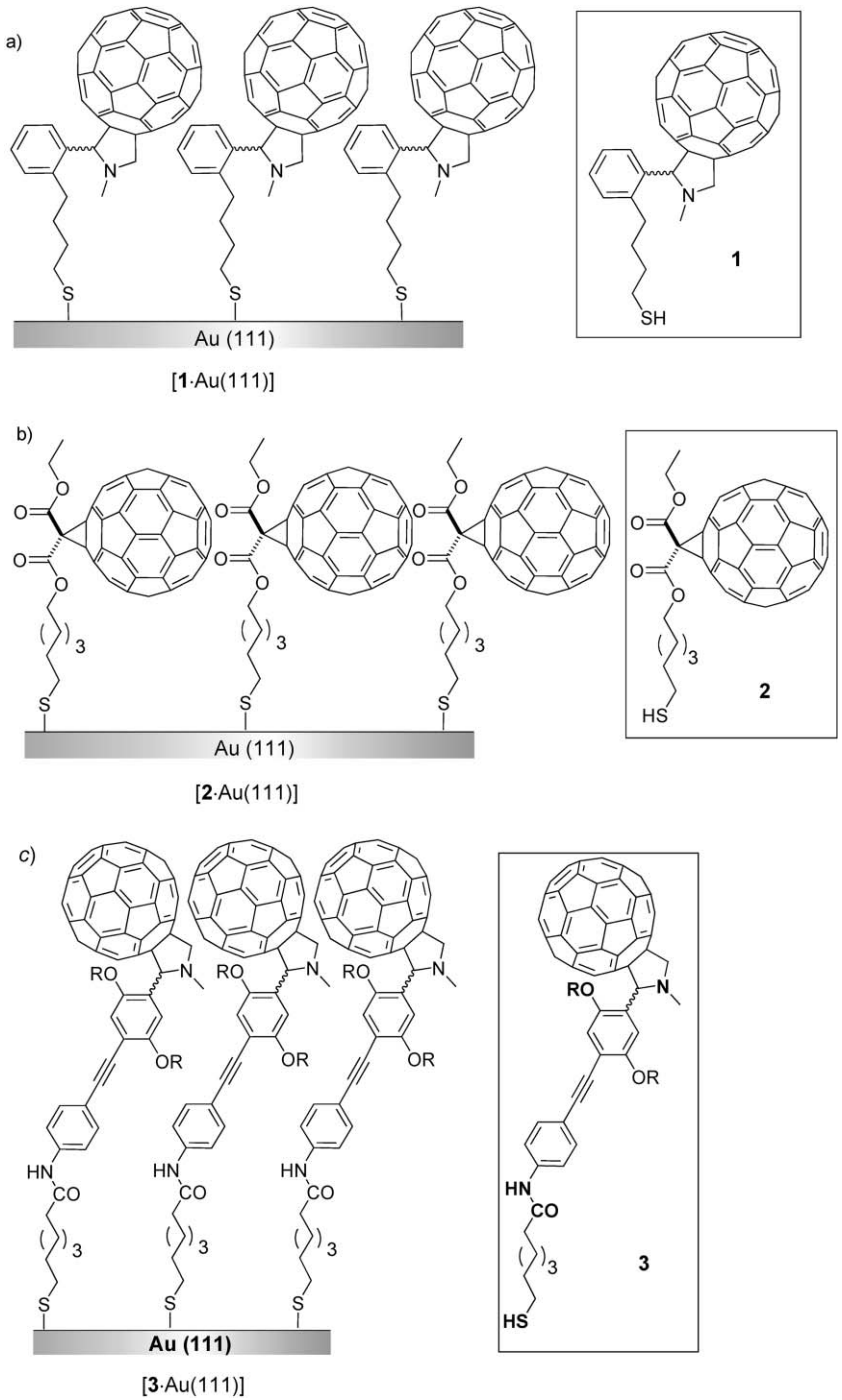


**Fig. 2** Schematic representation of SAMs of [60]fullerene derivatives bearing binding groups suitable for adsorption on Au(111) reported by a) Mirkin and co-workers,[36] b) Diederich and co-workers[42] and c) Fox and co-workers.[44]

consequences of the immobilisation of **1** on the Au surface. Very recently, derivative **1** was also self-assembled on thin mercury films (TMF) deposited on a glassy carbon electrode (GCE).[40] Two reversible, surface-confined redox couples were obtained for the [60]fullerene-containing [**1**·TMF/GCE] SAMs as studied by CV measurements in $CH_2Cl_2$. The surface coverage of [60]fullerene derivative **1** on TMF/GCE was measured to be in the range of 1.7–1.8 $\times$ $10^{-10}$ mole $cm^{-2}$, accounting for the formation of a full-coverage monolayer. Although in this case the substrate is a liquid, the first water contact angle measurements on Hg surfaces were performed, showing a dramatic enhancement of the surface hydrophobicity upon formation of the [60]fullerene-containing monolayer (from 61 $\pm$ 3° for bare Hg to 100 $\pm$ 3° for [**1**·TMF/GCE]).

In a collaborative work with the groups of Pretsch and Echegoyen, we applied a similar methodology to self-assemble [60]fullerene-derived thiol **2** on a Au(111) surface (Fig. 2b) for the fabrication of photoelectrochemical cells[41] and solid-contacted ion-selective electrodes (SC-ISEs)[42,43] (these applications will be discussed in Sections 4 and 5, respectively).

Surface-confined cyclic voltammetric measurements of the resulting monolayer on Au(111) revealed full coverage of the Au(111) surface ($\Gamma$(**2**) = 3.9 × $10^{-10}$ mol $cm^{-2}$). Next to CV measurements, the monolayer was also comprehensively characterised by ellipsometry, advancing contact angle and IR-spectroscopic measurements. Further improvements of the performance of the resulting devices were achieved by the formation of a mixed layer by insertion of *n*-octanethiol molecules in the preformed [60]fullerene-containing SAM ([$C_8H_{17}$S/**2**·Au(111)]). Although a loss of **2** ($\Gamma$(**2**) = 0.9 × $10^{-10}$ mol $cm^{-2}$) was detected, the mixed *n*-octanethiol-**2** film was found to be more stable due to an enhancement of the packing density of the underlying aliphatic chains as a consequence of the favourable filling of the free surface binding sites and of the empty space below the [60]fullerene cages in the SAM.

As observed for [**1**·Au(111)] SAMs, the presence of the bulky carbon cages favours the formation of interstitial holes within the monolayer leading to empty free spaces which are available for charge-compensating ions in electrochemical experiments. According to these structural requirements, Fox and co-workers prepared the self-assembled monolayer of [60]fullerene derivative **3** on Au(111) ([**3**·Au(111)], Fig. 2c).[44] The presence of pendant alkoxy chains on the phenyl rings produced very low-density monolayers as suggested by the measured surface coverage ($\Gamma$(**3**) ~ 0.99 × $10^{-10}$ mol $cm^{-2}$). Consequently, the low packing density allowed the incorporation of charge-compensating ions which is needed to satisfy the requirements for [60]fullerene dianion formation upon electrochemical reduction of the film. Cyclic voltammetric measurements showed two well-resolved reversible peaks ($E_{1/2}^{red,1}$ = −0.65 V and $E_{1/2}^{red,2}$ = −1.04 V; *vs.* Ag/AgCl) for the first and second [60]fullerene-centred one-electron reductions. Examples of other [60]fullerene conjugates (**4–9**) containing sulfur atoms utilised to form self-assembled monolayers on Au(111) surfaces are reported in Fig. 3.

Echegoyen and co-workers prepared self-assembled monolayers on Au(111) using (1,10-phenanthroline)-[60]fullerene derivative **10** (Fig. 4a) based on the strong interactions between the nitrogen atoms of the phenanthroline unit and the gold surface.[51] While [60]fullerene derivative **10** alone does not form a stable ordered SAM, very well ordered stacks were obtained when **10** was intercalated into a preformed 1,10-phenanthroline (**Phen**) monolayer. Mixed monolayer [**10**/**Phen**·Au(111)] owes its stability and order to the π–π interaction between phenanthroline moieties and the optimal distance between neighbouring carbon cages in the stacks. In contrast to the SAMs obtained with molecules **1**, **2** and **3**, compound **10** gave only a partial coverage of the Au surface, resulting in low-content fullerene monolayers. Similar SAMs have also been obtained by Zhu and co-workers, who coated Au(111) surfaces and gold nanoparticles with 2,2′-bipyridine- (**11**) and 2,2′:6′,2″-terpyridine-[60]fullerene (**12**) derivatives (Fig. 4b).[52] However, despite the high surface coverage, STM images showed the formation of 10 nm-sized aggregates accounting for the formation of structurally inhomogeneous monolayers.

**3.1.2 Strategy ii.** Following strategy *ii*, [60]fullerene-containing monolayers were obtained by *in-situ* bond-formation between $C_{60}$ and immobilised alkylamines on indium–tin-oxide (ITO) ($C_{60}$ → [$NH_2(CH_2)_3SiO_3$·ITO])[53] and on Au(111) ($C_{60}$ → [$NH_2(CH_2)_2$S·Au(111)], Fig. 5a).[54] The former amino-modified surfaces were obtained by chemisorption of

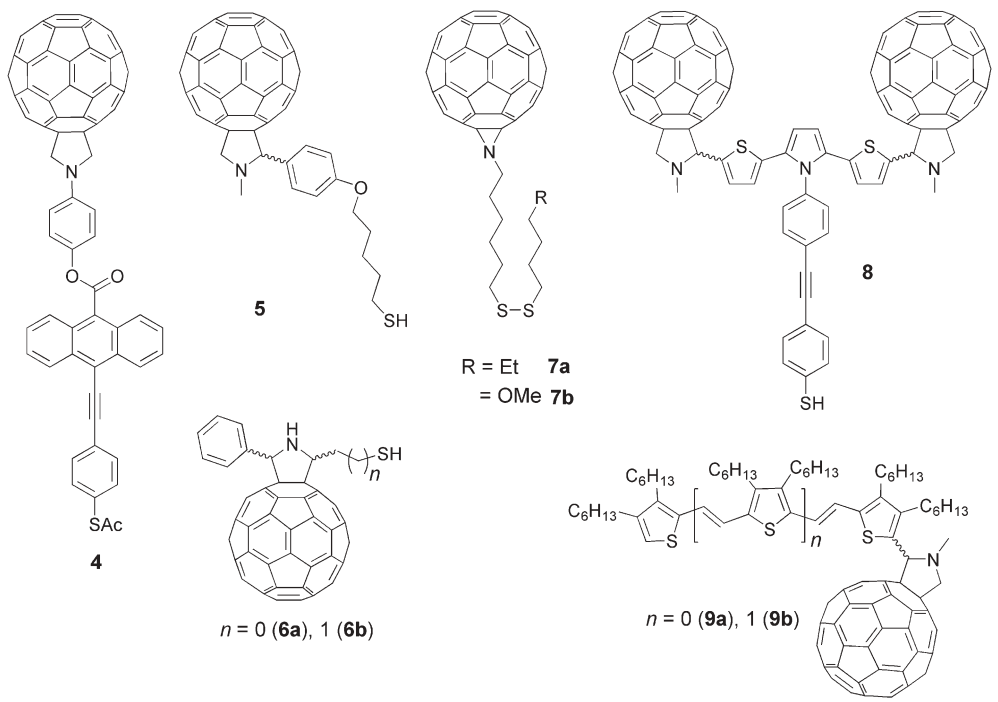


**Fig. 3** Molecular structures of acetyl-protected [60]fullerene-derived thiol **4**,[45] [60]fullerene-derived thiols **5**[46] and **6a–b**,[47] [60]fullerene-derived disulfides **7a–b**,[48] [60]fullerene-2,5-dithienylpyrrole triad **8**[49] and the two oligothiophene-[60]fulleropyrrolidine conjugates **9a–b**[50] utilized as precursors for the formation of stable SAMs on Au(111).

 

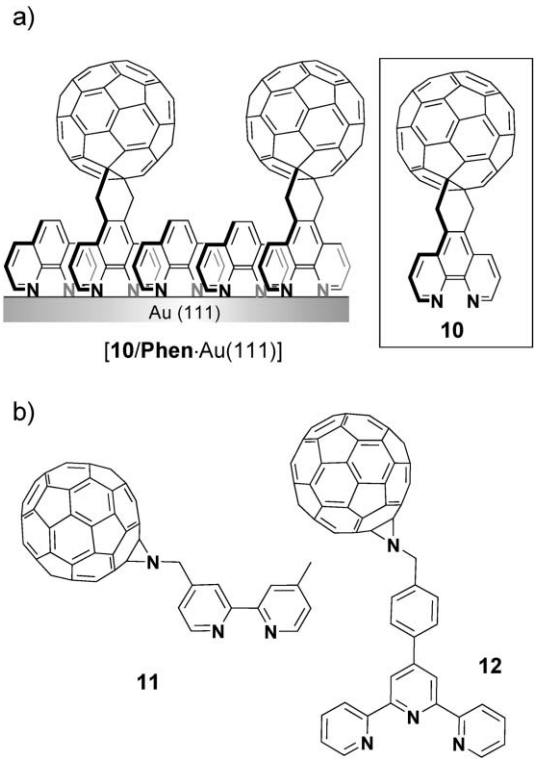


**Fig. 4** a) Schematic representation of a mixed SAMs of [60]fullerene derivatives **10** with 1,10-phenanthroline (**Phen**) on Au(111) as reported by Echegoyen and co-workers;[51] b) molecular structures of 2,2′-bipyridine- (**11**) and 2,2′:6′,2″-terpyridine-[60]fullerene (**12**) derivatives as reported by the group of Zhu.[52]

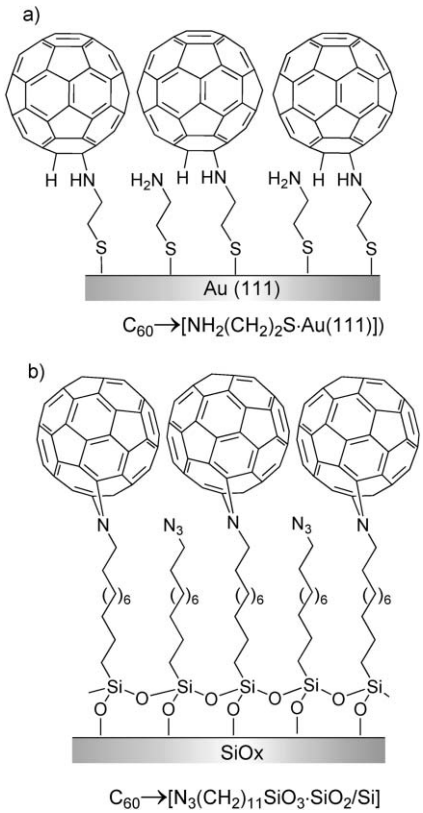


**Fig. 5** Surfaces covered with aliphatic residues bearing terminal amino[54] (a), and azido[55] (b) groups which undergo covalent bond formation with $C_{60}$. In this review, all $C_{60}$-containing SAMs prepared following strategy *ii* are named using the symbol "→", which indicates that pristine $C_{60}$ was reacted with an already preformed monolayer.

cysteamine on Au and $NH_2(CH_2)_3SiO_3$ on a base-treated ITO electrode, respectively. Both surfaces were fully characterised by X-ray photoelectron spectroscopy (XPS), electrochemistry, ellipsometry and water contact angle. In particular, both substrates revealed excellent surface coverage by $C_{60}$ ($\Gamma(C_{60})$ = $1.15 \times 10^{-10}$ mol cm$^{-2}$ and $1.7 \times 10^{-10}$ mol cm$^{-2}$ for $C_{60} \rightarrow [NH_2(CH_2)_2S{\cdot}Au(111)]$ and $C_{60} \rightarrow [NH_2(CH_2)_3SiO_3{\cdot}ITO]$, respectively). The RHN–$HC_{60}$ bond-forming reaction was confirmed by a cathodic shift ($\sim$30–50 mV) of the reductive half-wave potentials observed for $C_{60} \rightarrow [NH_2(CH_2)_3SiO_3{\cdot}ITO]$ ($E_{1/2}^{red,1} = -1.14$ V and $E_{1/2}^{red,2} = -1.51$ V *vs.* Fc/Fc$^+$) and pristine $C_{60}$ ($E_{1/2}^{red,1} = -0.98$ V and $E_{1/2}^{red,2} = -1.54$ V *vs.* Fc/Fc$^+$). On the basis of the electrochemical data for both $C_{60} \rightarrow [NH_2(CH_2)_2S{\cdot}Au(111)]$ and $C_{60} \rightarrow [NH_2(CH_2)_3SiO_3{\cdot}ITO]$ SAMs and several multiple adducts of $C_{60}$ with primary amines, the authors suggested that no more than two amino groups reacted with each carbon cage.

Following a similar strategy, Tsukruk, Lander and Brittain prepared [60]fullerene-containing monolayers reacting $C_{60}$ *in-situ* with azido functions immobilised on the surface through alkyl chains (Fig. 5b).[55,56] The azido-modified surface was obtained by chemisorption of (11-bromoundecyl)trichlorosilane onto $SiO_2$/Si wafers, followed by nucleophilic substitution of the bromide with $NaN_3$ (advancing water contact angle = 84 $\pm$ 1° and 80 $\pm$ 1° for $[Br(CH_2)11SiO_3{\cdot}SiO_2/Si]$ and $[N_3(CH_2)_{11}SiO_3{\cdot}SiO_2/Si]$ SAMs, respectively).[56] The functionalisation of the surface with $C_{60}$ was monitored by means of advancing water contact angle measurements ($70 \pm 1°$ for $C_{60} \rightarrow [N_3(CH_2)_{11}SiO_3{\cdot}SiO_2/Si]$). Atomic force microscopy (AFM) measurements revealed that the carbon cages are arranged in a face-centered cubic cell with an edge length $a$ of 1.4 $\pm$ 0.1 nm. The functionalised surfaces were then studied by friction force microscopy in order to unravel their nanotribological properties.[55] Velocity-dependent friction investigations revealed a non-monotonic behaviour which is related to the low exceeding energy dissipation produced by the intrinsic structural rearrangement of the carbon cage after force application.

Nevertheless, despite the excellent surface coverage and the ordered molecular packing as observed in the systems described in this subsection, strategy *ii* does not allow a strict control of the number of addends on the [60]fullerene carbon sphere, and thus definitely leads to a certain structural and physical inhomogeneity of the resulting SAMs.

### 3.1.3 Strategy iii.

*3.1.3.1Immobilisation of [60]fullerene derivatives via non-covalent interactions.* Pioneering work has been reported by the groups of Echegoyen and Kaifer who elegantly associated [18]crown-6-derived [60]fullerene **13** with a pre-organised self-assembled monolayer of ammonium ions on Au(111) (Fig. 6) through a tripod array of H-bonds in conjunction with ion–dipole interactions.[57] For this purpose, they synthesised [60]fullerene-crown ether adduct **13** which incorporates a

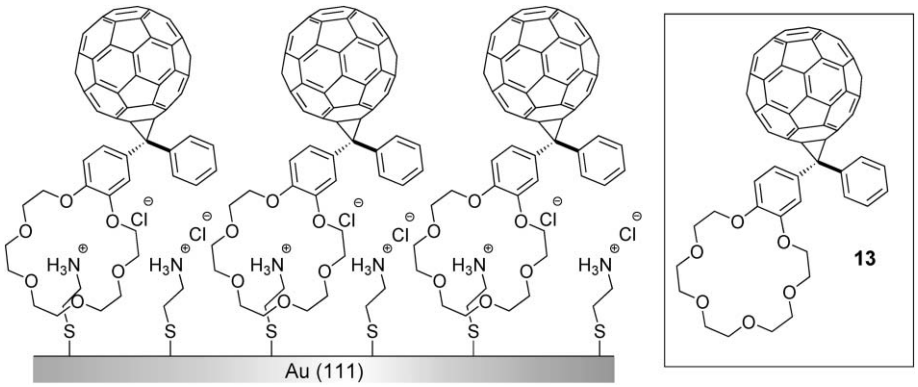


**Fig. 6** Supramolecular assemblies between fullerene-crown ether conjugate **13** and a positively charged SAM of alkylammonium ions.[57]

monobenzo-18-crown-6 moiety. A gold surface was chemically modified to support a thiolated SAM, formed of $Cl^{-}H_3N^{+}(CH_2)_2SS(CH_2)_2NH_3^{+}Cl^{-}$ molecules, which results in a surface fully covered by primary ammonium groups. When the modified gold layer was immersed into a $CH_2Cl_2$ solution of **13**, the surface became fully covered by a [60]fullerene monolayer. The non-covalent nature of the specific reversible (ammonium ion)–(crown ether) interaction between the ammonium-functionalised surface and **13** was confirmed by desorption experiments conducted in **13**-free solution. The close surface packing of the [60]fullerene moieties within the layer was demonstrated by Osteryoung square wave voltammetric measurements which revealed a surface coverage by **13** of $\sim 1.4 \times 10^{-10}$ mol cm$^{-2}$ (which is in agreement with the experimental values for a compact $C_{60}$ monolayer assuming a face-centred cubic packing, *cf.* above).

Supramolecular electrostatic-driven deposition of [60]fullerene derivatives on solid surfaces has been reported by Guldi, Prato and co-workers, who modified ITO surfaces *via* layer-by-layer (LBL) deposition of a [60]fullerene-donor dyad (Fig. 7).[58] Cationic [60]fullerene–tris(2,2′-bipyridine)ruthenium(II) complex **14** was adsorbed on an anion-covered ITO surface by Coulombic interaction taking advantage of the positively charged Ru(III)-complex moiety in the dyad. Anion coating of the ITO surface was achieved in two steps (Fig. 7): (step 1) anchoring of a base layer of poly(diallyldimethylammonium) (PDDA) onto the hydrophobic surface *via* simple polymer spin-coating followed by the deposition (step 2) of a poly(styrene-4-sulfonate) (PSS) bearing anionic sulfonate functionalities. The resulting modified surfaces were sufficiently covered with negative charges that molecule **14** was easily deposited by immersing the substrate into an organic solution of the dyad (step 3, Fig. 7). Sequential repetition of steps 2 and 3, namely the deposition of polymer PSS and dyad **14**, led to the formation of a multilayered material of controlled thickness and composition. The multilayered deposition process was easily monitored by UV-Vis spectroscopy, which showed a progressive increase in the fullerene absorbance intensity upon increasing the number of layers. Although this strategy exhibits some limitations caused by the unavoidable interpenetration of the adjacent layers, this methodology could constitute a valid alternative to traditional techniques toward the fabrication of [60]fullerene-based photovoltaic cells since the photocurrent response can be easily tuned by varying the number of deposited bilayers.[12,59]

*3.2.3.2 Covalent immobilisation.* Gulino, Fragalà and co-workers prepared [60]fullerene-containing monolayers ([**15**-$CH_2C_6H_4SiO_3{\cdot}SiO_2$], Fig. 8) on silica surfaces by covalently reacting [60]fullerene derivative **15**, bearing a phenolic

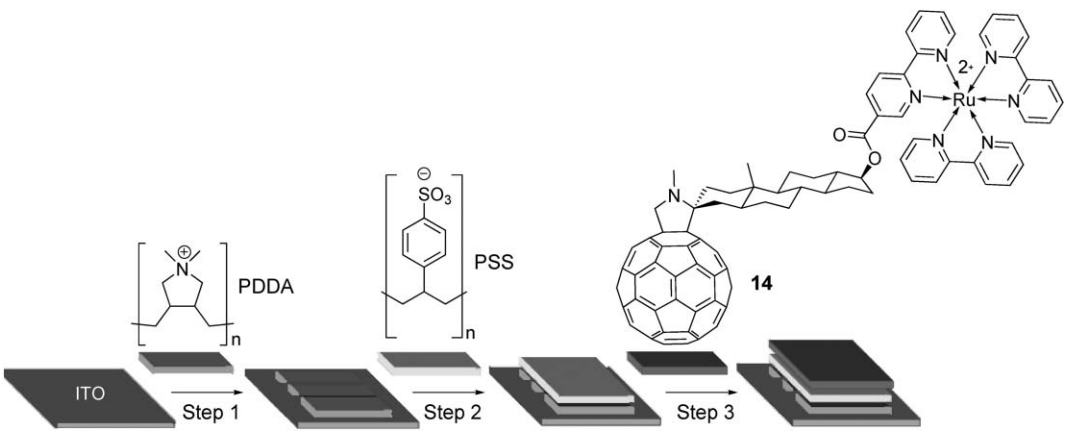


**Fig. 7** Schematic illustration of the preparation of a monolayer of [60]fullerene–tris(2,2′-bipyridine)ruthenium(II)complex **14** following the LBL methodology: step 1, deposition of PDDA; step 2, deposition of PSS; step 3, deposition of the cationic [60]fullerene derivative **14**.[12]

 

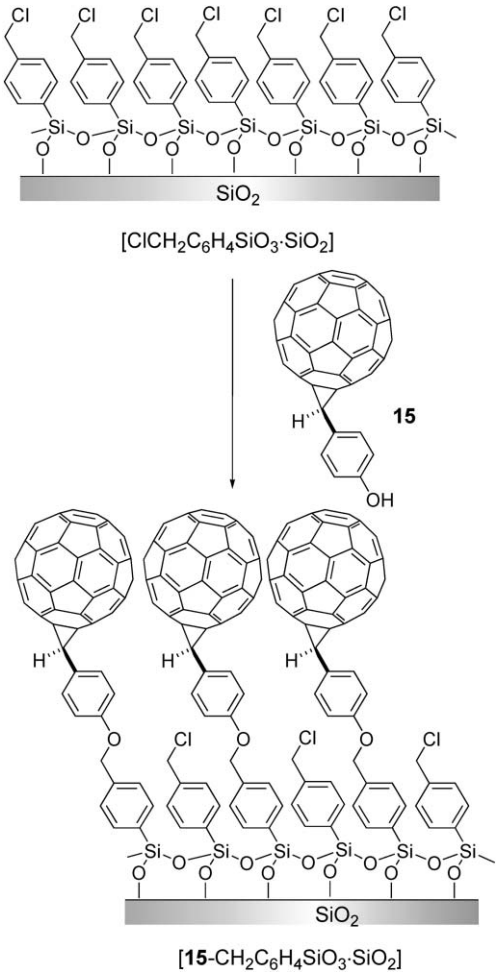


**Fig. 8** Covalent functionalisation of Cl-terminated silica surfaces with (*p*-hydroxyphenylmethano)fullerene derivative **15**.[60]

moiety, with a [4-(chloromethyl)phenyl]silane-terminated silica surface ([$ClCH_2C_6H_4SiO_3{\cdot}SiO_2$]).[60] By means of both static and dynamic contact angle measurements, the authors confirmed the [60]fullerene immobilisation by measuring the enhanced hydrophobic character of the surface, which was revealed to increase considerably after the carbon sphere linkage (5°, 79° and 82° for clean $SiO_2$, [$ClCH_2C_6H_4SiO_3{\cdot}SiO_2$] and [**15**$\cdot CH_2C_6H_4Si{\cdot}SiO_2$], respectively). In a comprehensive use of angle-resolved XPS spectroscopy, the surface atomic composition of both modified silica substrates [$ClCH_2C_6H_4SiO_3{\cdot}SiO_2$] and [**15**-$CH_2C_6H_4SiO_3{\cdot}SiO_2$] has been fully investigated. Specifically, upon reaction of the [$ClCH_2C_6H_4SiO_3{\cdot}SiO_2$] SAM with alcohol **15**, the C(1s) peak and a weak unresolved Cl(2p) doublet appeared at 285.0 and 199.5 eV binding energies, respectively. Both carbon and chlorine atomic concentrations show a monotonic increase upon decreasing the photoelectron takeoff angles (C being 24.0% and Cl being 0.08% at 45°, 30.5% and 0.10% at 30°, 50.0% and 0.13% at 15° and 64.2% and 0.28% at 5°) confirming the upper layer carbon-based nature of the signal and the quasi total disappearance of the Cl functions. To further investigate the thickness of the [**15**-$CH_2C_6H_4Si{\cdot}SiO_2$] assembly, atomic force lithography was performed. Surface-confined molecules were removed along a straight line by scratching the surface with the AFM tip under a suitable constant force. The deepness of the scratch obtained for [**15**-$CH_2C_6H_4Si{\cdot}SiO_2$] was measured to be *ca.* 19 Å, which is in good agreement with the estimated value of the molecular height (19.8 Å) as calculated in computing simulation using a molecular mechanics force field (MM+).

**3.2.4 Strategy *iv*.** All previously described strategies, accomplish the formation of [60]fullerene-containing SAMs *via* attachment of chemically modified [60]fullerene derivatives, which involves a partial destruction of the π-delocalisation in the carbon sphere as a result of the attachment of a pendant addend. Strategy *iv* is concerned with the non-covalent immobilisation of pristine $C_{60}$ onto surfaces. The first example has been reported by Shinkai and co-workers, who prepared ultra-thin $C_{60}$-containing layers on an Au(111) surface capitalising on the self-assembly between a hexacationic calix[3]arene cage and the $C_{60}$ sphere that leads to the capsular 2:1 host–guest inclusion complex **16**.[61,62] Deposition of the $C_{60}$–calix[3]arene complex on a Au(111) surface with an anionic coating yielded the SAM schematised in Fig. 9. The surface coverage was estimated to be $\sim 1.7 \times 10^{-10}$ mol cm$^{-2}$ and $\sim 1.4 \times 10^{-10}$ mol cm$^{-2}$ by means of CV measurements and UV-Vis absorption spectroscopy, respectively. This SAM showed also a photoelectrochemical response under visible light irradiation ($300 < \lambda < 510$ nm) due to an electron transfer occurring from the excited triplet state of $C_{60}$ ($^3C_{60}$*) to the Au electrode. Deposition of an anionic sulfonated porphyrin-containing polymer on a **16**-containing SAM placed on an ITO electrode led to hybrid films generating a photocurrent response with high quantum yields (21%).[62]

The group of Echegoyen described an alternative methodology to confine pristine $C_{60}$ onto surfaces by combining a defined molecular recognition event (the complexation between $C_{60}$ and a cyclotriveratrylene (CTV) host) with the formation of a self-assembled monolayer.[63,64] For this purpose, CTV derivatives bearing disulfide (**17**) and thioether functionalities (**18**) have been synthesised (Fig. 10a). Gold electrodes were chemically modified with CTVs **17** and **18** to support thiolated SAMs displaying CTV-capped hollow spaces. Both [**17**·Au(111)] and [**18**·Au(111)] SAMs have been extensively characterised by CV blocking experiments (monitoring the response of the $[Ru(NH_3)_6]^{3+/2+}$ redox couple), impedance spectroscopy and electrochemical reductive desorption. SAMs of [**17**·Au(111)] exhibited a better blocking behaviour and a higher surface coverage than those of **18**, as a consequence of the stronger binding affinity between the cyclic disulfide residues and the Au surface. Studies of non-covalent immobilisation of $C_{60}$ on the modified surfaces have been performed immersing both SAMs in a 1,2-dichlorobenzene solution of $C_{60}$ for 10 h. Two well-resolved reversible redox waves for the first and second reduction processes ($E_{1/2}^{red,1} = -0.93$ and $E_{1/2}^{red,2} = -1.34$ V *vs.* Ag/AgCl in $CH_3CN$) were observed in the case of [**17**·Au(111)] SAMs, clearly showing the presence of $C_{60}$. All peaks revealed to be slightly broad, suggesting different interacting modes between the fullerene cages and SAM [**17**·Au(111)], namely through encapsulation of the $C_{60}$ molecules in the CTV-capped cavities (see a

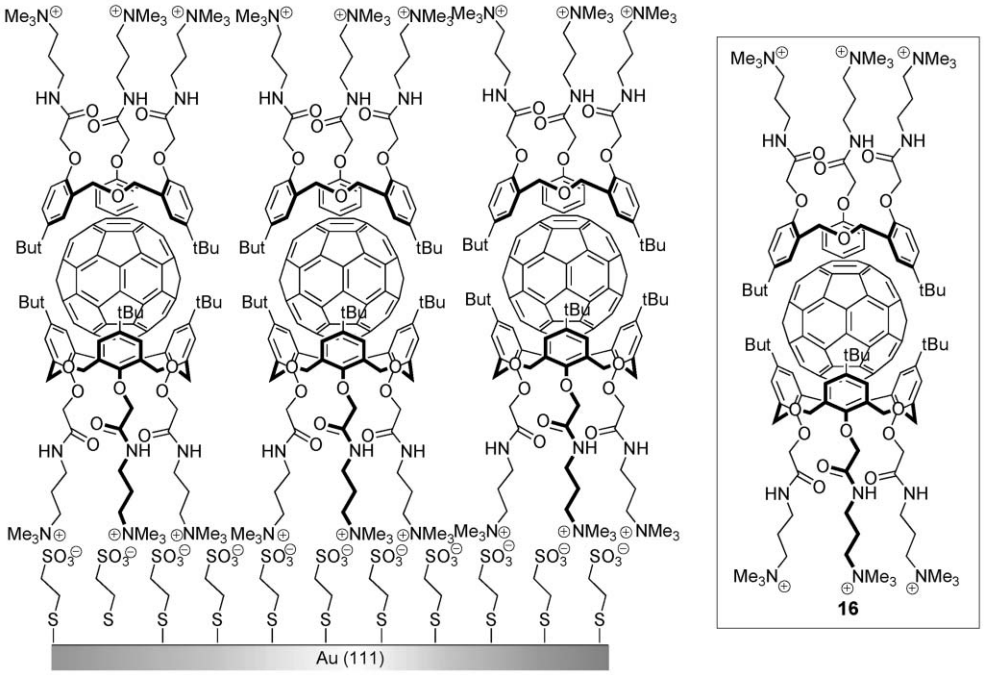


**Fig. 9** $C_{60}$-containing thin films obtained by assembly of a hexacationic homooxacalix[3]arene-$C_{60}$ 2:1 host–guest complex (**16**) and an anion-coated Au(111) surface.[61]

schematic example displayed in Fig. 10b) or by intercalation into the voids between the adsorbed CTV molecules.

Surprisingly, SAMs of **18** were unable to bind $C_{60}$ under the same complexation conditions. Nevertheless, if the Au surface was kept in the solution containing both $C_{60}$ and **18** molecules for two weeks, the resulting [**18**·Au(111)] SAM did show a partial immobilisation of $C_{60}$ as shown by CV measurements (fullerene-centred $E_{1/2}^{red,1} = -0.93$ and $E_{1/2}^{red,2} = -1.34$ V *vs.* Ag/AgCl in $CH_3CN$). These results, indicates that the binding of $C_{60}$ into SAMs of **18** appears to be kinetically disfavoured probably due to the presence of long aliphatic chains that point outside the cavity occluding the accessibility to the hollow space and thus reducing its binding ability. The same authors further explored the non-covalent immobilisation of $C_{60}$ in preorganised porphyrin-capped cavities formed by self-assembly of tetrapyrrolic macrocyles functionalised with four cyclic alkyldisulfide legs on gold surfaces as in **17**.[64,65] Although the attractive interaction between $C_{60}$ and porphyrins is known to be more effective than that with CTVs as a consequence of more favourable π–π donor–acceptor interactions, such porphyrin-based SAMs unexpectedly revealed to scarcely bind $C_{60}$ suggesting that some geometrical requisites, *i.e.* a preorganised cavity, are missing. Presumably, the flat porphyrin interacts too strongly with the surface leading to the collapse of any possible cavity.

In very elegant work, the groups of Beton and Champness described another approach to prepare highly ordered assemblies of pristine $C_{60}$ by constructing a two-dimensional pre-organised monolayer featuring empty domains that can host fullerene cages.[66] For that purpose, they prepared a two-dimensional honeycomb-like network by UHV co-deposition of 3,4,9,10-perylenetetracarboxylic diimide (PTCDI) and 2,4,6-triamino-1,3,5-triazine (melanine) on a Ag-terminated silicon surface. As shown by detailed STM images, the two molecular modules organise in such way that hexagonal domains are formed. The vertices and the straight edges are constituted by the melanine and PTCDI modules, respectively. The self-assembly is driven by intermolecular triple hydrogen-bonding interactions that are established between the two molecular components. Subsequently, pristine $C_{60}$ was evaporated on top the honeycomb networks, thereby forming a hybrid fullerene monolayer on the surface of the nanostructured preorganised PTCDI–melanine assembly. As shown by STM measurements, the fullerene cages are hosted inside the hexagonal cavities as heptameric clusters. Mere deposition of pristine $C_{60}$ on the same surface led to the formation of extended monolayers and multilayered islands, but never isolated hexagonal-like heptameric fullerene clusters. These observations clearly exclude any substrate influence on the fullerene organisation, thus demonstrating that the formation of the heptameric clusters is solely templated by the underlying PTCDI–melanine supramolecular network.

Following a similar strategy, we showed that thermal evaporation of a sub-monolayer of porphyrin **19** onto Ag(111) surfaces affords at room temperature self-organised nanostructured monolayers.[67,68] The extended structure revealed the presence of very regular domains of empty pores (with inter-pore distances of *ca.* 3.4 nm) with nano-dimension (*ca.* 1.2 nm in diameter) (see inset Fig. 11). Successive thermal evaporation of $C_{60}$ led to the formation of a hybrid supramolecular monolayer in which the carbon cages are hosted inside the pores (Fig. 11a–b). Very interestingly, the $C_{60}$-pore ''inclusion complexes'' interact/communicate with their neighbours leading to the formation of chains and islands of $C_{60}$ around initially filled pores (Fig. 11c–d). Remarkably, the distances ($\sim$3.4 nm) between single $C_{60}$ molecules trapped in

 

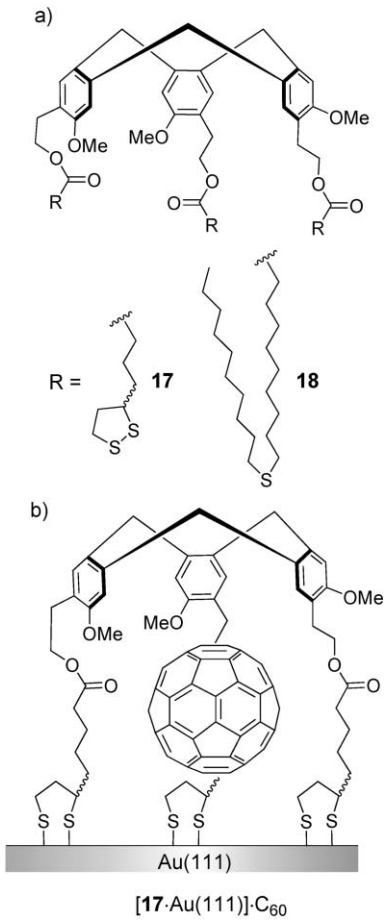


**Fig. 10** a) Molecular structures of the disulfide-bearing cyclotriveratrylene (CTV) derivatives **17** and **18** utilised for the non-covalent encapsulation of $C_{60}$ on gold surfaces;[63] b) schematic representation of the proposed cyclophane-type geometry for the surface-confined encapsulation of $C_{60}$ within a SAM of **17** ([**17**·Au(111)]·$C_{60}$).

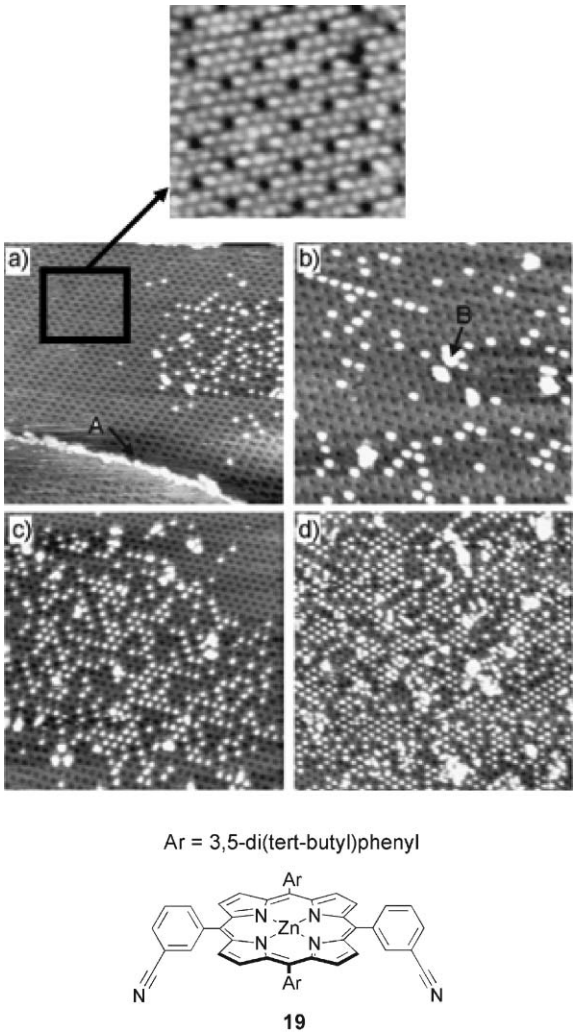


**Fig. 11** STM images of the hybrid **19**-$C_{60}$ assembly at different $C_{60}$ coverage: 0.02 ((a) and (b), scan range: 93 × 88 $nm^2$ and 68 × 64 $nm^2$, respectively), 0.07 ((c), scan range: 100 × 100 $nm^2$) and 0.1 ((d), scan range: 111 × 112 $nm^2$).[67] Inset: STM image of a SAM of porphyrin **19** deposited on Ag(111) showing (left) empty receptor sites (black spots). In Fig. 11a–d, the hosted fullerenes appear as white spots. Some aggregation is also observed at surface steps and/or defects (arrow in (b)). At high $C_{60}$ coverage (d), the majority of the hosting cavities are occupied by the carbon cages. Reprinted with permission from reference 67.

the pores remained very large (more than the van der Waals distance) excluding any sort of through-space $C_{60}\cdots C_{60}$ interactions. As clearly shown by time-lapsed series of images of the $C_{60}$–porphyrin assembly, the guest fullerene molecules are not sitting permanently on the initial position, but rather they move within the porous network.[69] This implies an attractive long-range mechanism between the guest molecules which is partially mediated by the conformational mobility of the porphyrin molecules constituting the patterned monolayer.

## 4. Light-harvesting devices incorporating [60]fullerene-based monolayers

$C_{60}$ and its derivatives are appealing components to be incorporated in functional materials because of the exceptional electron-accepting and low-lying level of the excited states.[4,6] Upon UV-Vis irradiation, the ground state of $C_{60}$ is excited to its first singlet state, $^1C_{60}$ ($\tau$ = 1.3 ns) which rapidly decays in near-quantitative yield ($\Phi \approx 0.96$) to the triplet excited state, $^3C_{60}$ ($\tau$ = 135 μs), thanks to an efficient intersystem crossing (ISC). $^3C_{60}$ is the longest-lived as well as the lowest-lying excited state (1.56 eV), so that deactivation pathways, which are competing with the non-radiative transition to the ground state, generally emanate from $^3C_{60}$ as the excited state. $^3C_{60}$ can be deactivated through energy transfer or through photoinduced electron transfer from an electron donor (D) species, yielding the radical anion $C_{60}^{\bullet -}$ and the radical cation $D^{\bullet +}$.[5,70] The latter phenomenon is the most appealing physical property in the field of [60]fullerene photochemistry. In fact, the exceptionally small reorganisation energy (between ~0.7 and ~0.3 eV depending on the solvent) which mainly consists of solvent reorganisation, drives the photoinduced electron transfer from the ''normal region'' close to the ''top region'' and the back electron transfer (charge recombination) into the Marcus ''inverted region''. Experimentally, this means that all [60]fullerene-containing donor–acceptor dyads possess, upon

photoexcitation, a long-lived charge separated (CS) state because of the acceleration and deceleration of the charge separation and recombination rates, respectively. In line with such an approach, a large number of donor-functionalised [60]fullerenes incorporated in well-defined two-dimensional and three-dimensional networks have been synthesised in the last decades.[12,71] Most of these systems have been engineered to mimic natural photosynthetic processes such as light harvesting and charge separation.[72] Among all possible [60]fullerene–donor dyads, [60]fullerene–porphyrin conjugates have been the most widely investigated photoreaction systems due to the extremely small reorganisation energy during photoinduced electron transfer—estimated to be in the 0.23–0.5 eV range, depending on the precise chemical structure of the [60]fullerene–porphyrin conjugate.[73]

### 4.1 Light conversion into electrical energy: towards applications in solar energy conversion

In order to exploit the potential properties of molecular photosynthetic reaction centres in real working devices, the molecules must be confined on a surface of an electrode which, which in turn, should be able to collect the electrons. The organisation of photo-functional molecular assemblies on an electrode is a critical aspect which needs to be addressed in order to optimise the device performance. In this respect, it is of prime importance to reproducibly control the organisation of the molecular architectures on the surfaces in order to investigate their photochemical activities as ''organised molecular aggregates''. Therefore, the practical development of organic photovoltaic devices necessitates the synthesis of photofunctional molecules that possess all necessary physical and structural prerequisites to uniformly cover the electrode surface. In particular, a large number of attempts towards the preparation of photocurrent conversion devices has actually been performed using SAM techniques, mainly following the strategies *i*, *iii* and *iv* (Fig. 1) described in Section 3 of this review. In this context, Imahori and co-workers reported the first example of a [60]fullerene dyad for the construction of solar energy conversion devices that mimic the primary electron transfer events in photosynthesis.[74] Accordingly, they reported the first spontaneous self-assembly of a [60]fullerene/porphyrin-based donor–bridge–acceptor dyad (**20**), bearing a thioether group at the porphyrin moiety, on an Au surface (Fig. 12). Electrochemical studies and advancing contact angle measurements showed that the SAM presents a loosely packed structure on the gold electrode. Upon illumination of this photosensitive dyad monochromatic light ($300 < \lambda < 700$ nm) in argon-saturated $Na_2SO_4$ solution containing methyl viologen ($MV^{2+}$) as an electron carrier, the authors detected a short-circuit cathodic photocurrent in the sub-μA $cm^{-2}$ range, and calculated the quantum yield for photoinduced electron transfer to be *ca.* 0.5%. As a result of photophysical solution phase studies on **20**, the cathodic photocurrent generation (Fig. 12) in the photoelectrochemical cell is believed to be associated with a photoinduced electron transfer from the excited singlet state of the zinc porphyrin moiety (Zn) to the fullerene moiety resulting in a charge-separated state $ZnP^{\bullet+}$–$C_{60}^{\bullet-}$. In the next step, the [60]fullerene radical anion transfers an electron to the diffusing electron carrier $MV^{2+}$, which eventually passes it on to the counter electrode.

The same authors showed that a SAM prepared on a gold electrode from a $C_{60}$-derived thiol bearing a thioalkane moiety alone (**21**), is suitable for the generation of a stable anodic photocurrent under illumination and in the presence of an electron sacrificer such as ascorbic acid (Fig. 13).[75] The anodic photocurrent suggests the generation of a vectorial electron flow from the electron sacrificer to the gold electrode *via* the excited states of the photoactive $C_{60}$ core with a quantum yield of *ca.* 10%. A substantial improvement in the performance of this photoelectrochemical cell could be observed as compared to the previous system where the porphyrin is thought to be the primary photoactive chromophore in the multistep photoinduced electron transfer.

Employing a similar strategy, we also observed a photoelectric response upon exposure of a SAM of [**2**·Au(111)] to ambient light.[41] This observation led us to develop two photoelectrochemical cells based on SAM [**2**·Au(111)] with and without a cast polyurethane-based membrane. Both systems showed immediate and reversible anodic short-circuit photocurrent and open-circuit photovoltage upon illumination of the modified gold electrodes. Characterisation of the photoelectrochemical cells by recording the action spectra and atmosphere-alert *I*/*V* curves demonstrated that a photoinduced electron transfer occurs through the $C_{60}$-containing SAMs, acting as the photoactive species, to the gold electrodes. Deposition of a polyurethane membrane on the fullerene-containing SAM was shown to successfully improve steadiness

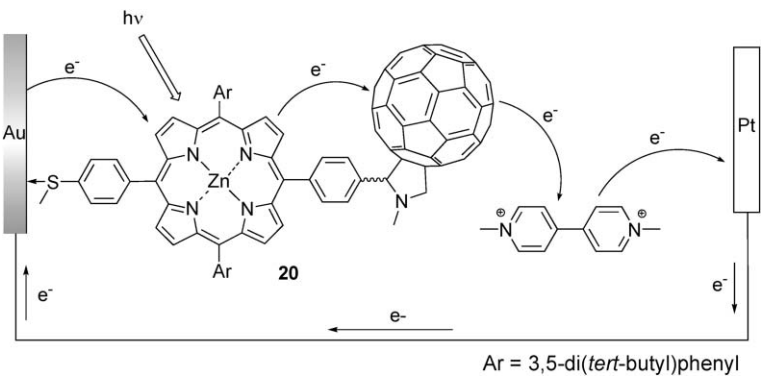


**Fig. 12** Photoinduced multistep electron transfer at a gold electrode modified with a SAM of porphyrin–$C_{60}$ dyad **20**.[74]

 

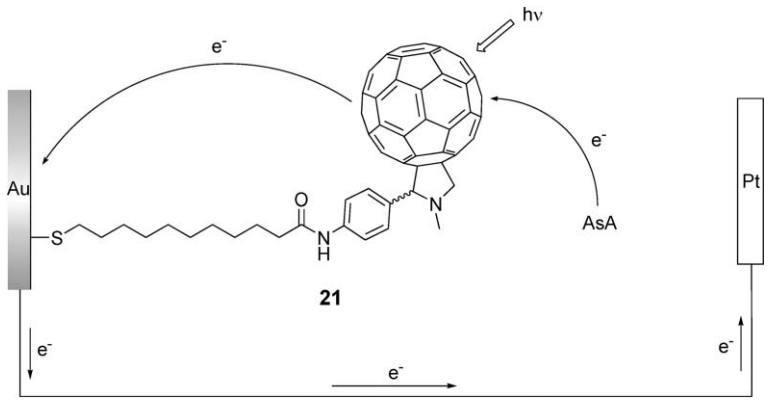


**Fig. 13** Photoinduced multistep electron transfer at a gold electrode modified with a $C_{60}$-containing SAM (AsA = ascorbic acid).[75]

and efficiency of the photoelectric response under unbiased conditions, indicating that the utilisation of a cast solvent-polymeric membrane has a favorable effect on the light conversion efficiency and might constitute a novel and original approach to increase the stability and efficiency of such cells. On the other hand, the photocurrent was found to be reduced compared to the device lacking the polyurethane-based membrane when a positive bias was applied in the presence of $O_2$. The two photoelectrochemical cells exhibited very high quantum yields (between 25 and 31%) for photoinduced electron transfer. These investigations led to the establishment of a mechanism for photocurrent generation in which water is proposed to be the ultimate electron donor, thereby offering potential for the prospects of photoelectrocatalytic systems for water splitting.

Imahori, Sakata *et al*. have extended these systems and developed the first artificial photosynthetic cell based on a gold electrode modified with a SAM of a ferrocene–porphyrin–$C_{60}$ triad (**22**, Fc–P–F, Fig. 14).[76] The energy levels of each state in the triad were carefully chosen and are in the order $Fc–{}^1P^*–F > Fc–P^{\bullet+}–F^{\bullet-} > Fc^{\bullet+}–P–F^{\bullet-}$. The SAM of the triad on a gold electrode was electrochemically characterised to be well-packed with almost perpendicular orientation of the triad with respect to the electrode surface. A cathodic photocurrent, which increases with an increase of the negative bias, was observed during the irradiation of the modified gold electrode implying an electron flow from the gold electrode to the counter electrode through the electrolyte. Under optimal conditions, the quantum yield was found to be 25% which was, at this time, the highest value ever reported for photosynthetic electron transfers across artificial membranes or at monolayer-modified metal electrodes. The photocurrent generation has been explained as follows: photoinduced electron transfer takes place from the excited singlet state of the porphyrin to the [60]fullerene moiety. The resulting [60]fullerene-centred radical mono-anion cedes an electron to diffusing electron carriers such as oxygen and/or methyl-viologen, which eventually transfer an electron to the counter electrode. On the other hand, an electron migration occurs from the gold electrode to the porphyrin radical cation *via* the ferrocenyl moiety, thereby restoring the initial state. These results prove that, in order to obtain efficient photoinduced multistep electron transfer at a modified gold electrode, the initial photoinduced electron transfer from the donor to the first acceptor must compete with the deactivation of the excited state by the gold electrode. In addition, the charge shift from the acceptor to the diffusing electron carriers or from the donor to the acceptor radical cation must be much faster than

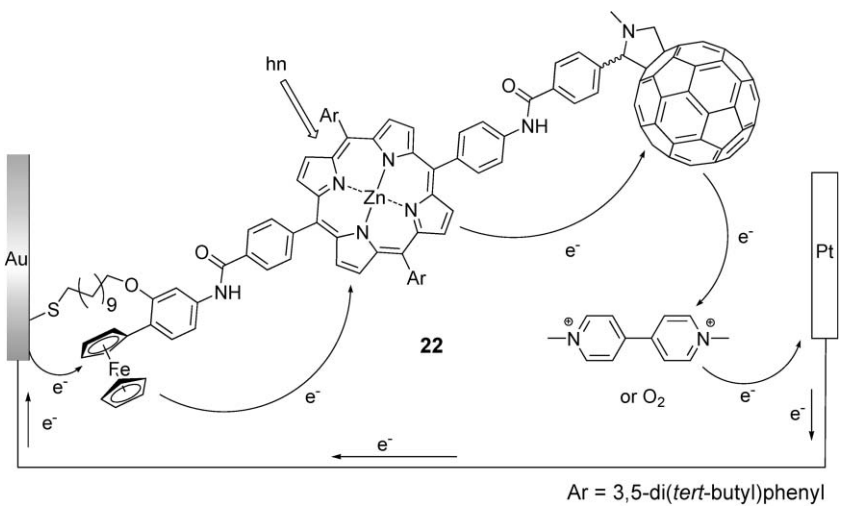


**Fig. 14** Photoinduced multistep electron transfer at a gold electrode modified with a SAM of a ferrocene–porphyrin–$C_{60}$ triad.[76]

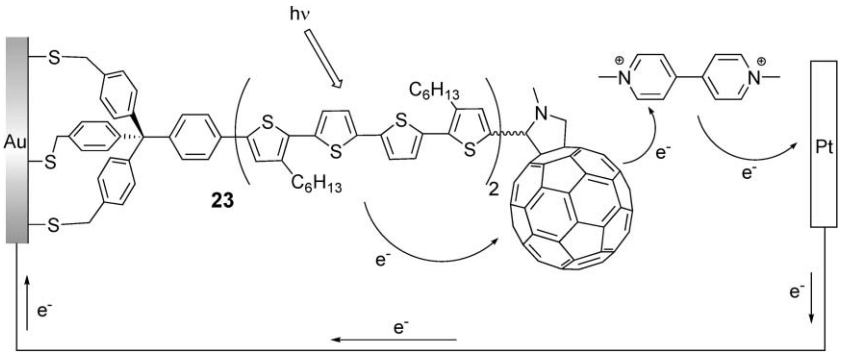


**Fig. 15** Photoinduced multistep electron transfer at a gold electrode modified with a SAM of quaterthiophene–$C_{60}$ dyad **23**.[78]

the charge recombination to the ground state. As development of this pioneering work, other ferrocene–porphyrin–fullerene triad conjugates grafted to Au(111) and ITO surfaces for solar energy conversion systems have also been reported recently by the same authors.[77]

Fukuzumi and co-workers reported a very large photocurrent generation in a photoelectrochemical cell based on a SAM of a [60]fullerene-linked oligothiophene (**23**) bearing a tripodal rigid binding group (Fig. 15).[78] This anchor, a tetraphenylmethane derivative having three sulfanylmethyl ''arms'', was shown to play a primordial role in the self-assembly of the adsorbate into a well-organised and robust monolayer on gold. On the basis of the reported photodynamics of the oligothiophene–[60]fullerene dyad, together with the results on similar photoelectrochemical cells, the authors concluded that photoexcitation of the quaterthiophene chromophore first induces electron transfer from this moiety to the [60]fullerene to generate a net vectorial electron flow from the gold cathode to the Pt counter electrode *via* the $MV^{2+}/MV^{+}$ redox couple under an applied potential bias (Fig. 15). The remarkably large quantum yield ($35 \pm 8\%$) observed for this system indicates that oligothiophenes can facilitate the generation and charge transport of a photocurrent.

Very recently, Kim, Park and co-workers reported an elegant approach to prepare highly ordered photoactive SAMs by a templated functionalisation of ITO surfaces exploiting the coordinating properties of a Zn–porphyrin moiety.[79] Specifically, the novel [60]fullerene–porphyrin dyad structure $Os_3(CO)_7(CNR)(CNR')(\mu^3\text{-}\eta^2\text{:}\eta^2\text{:}\eta^2\text{-}C_{60})$ (**24**, R = $(CH_2)_3Si(OEt)_3$, R′ = ZnP) (Fig. 16) in which a tri-osmium carbonyl cluster moiety links a [60]fullerene moiety, a porphyrin unit and a 3-(triethoxysilyl)propyl isocyanide, was grafted on an ITO surface in the presence of diazabicyclooctane (DABCO). The DABCO molecule induces pairs of neighboring porphyrins at the dyad termini to come in close proximity, thereby considerably reducing the surface area occupied by each conjugate. This coordination effect was confirmed by electrochemical surface-coverage measurements, which showed that the surface coverage of the **24**-based SAM prepared in the presence of the DABCO template ([DABCO·**24**·ITO]) was three time higher than that without ([**24**·ITO]) ($\Gamma$(**24**) = $1.8 \times 10^{-10}$ mol $cm^{-2}$ and $0.6 \times 10^{-10}$ mol $cm^{-2}$, respectively). The CV of [DABCO·**24**·ITO] revealed three well-resolved redox waves at −1.17, −1.47 and −1.92 V ($E_{1/2}$ *vs.* $Fc/Fc^{+}$) with relative areas of 1 : 1 : 3, of which the first and second waves correspond to the first two fullerene-centred one-electron reductions while the third wave

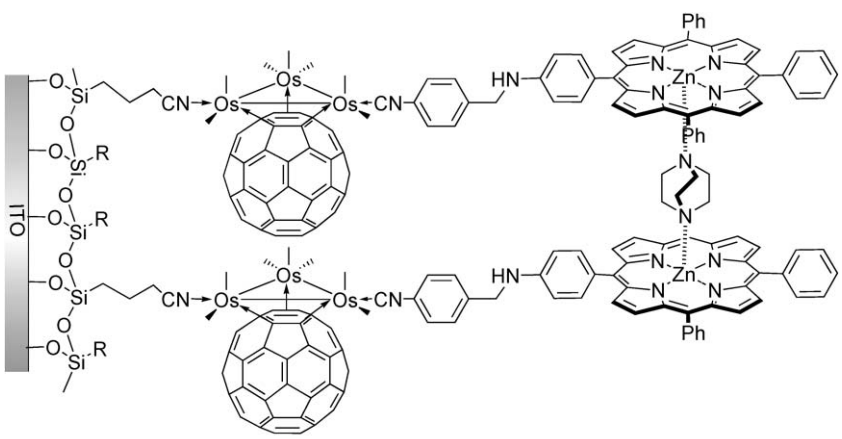


**Fig. 16** ITO electrode modified with a 3-(triethoxysilyl)propyl isocyanide linking a tri-osmium carbonyl cluster moiety complexed to a [60]fullerene and a porphyrin unit ([DABCO·**24**·ITO]).[79] The CO ligands to the Os centres are not shown for clarity.

 

corresponds to an overlapping between two reduction processes: a two-electron reduction centred on the [60]fullerene–triosmium cluster moiety and a one-electron reduction of the porphyrin moiety. Photocurrent measurements for SAMs were carried out using ascorbic acid (AsA) as a sacrificial electron donor. The quantum yields for the [**24**·ITO]/AsA/Pt and [DABCO·**24**·ITO]/AsA/Pt cells were estimated to be in the order of 10 and 19%, respectively. Transient absorption measurements acquired at 27 ps time delay for SAM [DABCO·**24**·ITO] revealed the presence of a positively charged porphyrin–DABCO complex cation with *ca.* 27 ps rise and a few hundred picosecond decay time. The delocalisation of the positive charge over both moieties slowed the charge recombination rate thus leading to an exceptional enhancement of the photocurrent generation efficiency.

Thomas, Kamat and co-workers prepared a self-assembled photoactive antenna system containing gold nanoparticles as central nanocores and appended $C_{60}$ moieties as the photoreceptive hydrophobic shells by functionalising the gold nanoparticles with a thiolate derivative of $C_{60}$ (**5**, Fig. 3).[46] Upon suspension of the [60]fullerene-functionalised gold nanoparticles stabilised by addition of dodecanethiol molecules ([$C_{12}H_{25}$S/**5**·Au], size ~3 nm) in toluene, the authors observed the formation of clusters of 5–30 nm in diameter. The ease of suspending these nanoassemblies in organic solvents allowed the determination of the excited state interactions between carbon cages by spectroscopic methods. The fluorescence quenching as well as decreased yields of the [60]fullerene triplet excited state suggested the participation of the singlet excited state of the [60]fullerene units in an energy transfer process to the gold nanocores. Electrophoretic film casting of the [$C_{12}H_{25}$S/**5**·Au] nanoassemblies on an optically transparent electrode (OTE) yielded a photoelectrochemical cell (Fig. 17) in which the photoactive [60]fullerene-derived systems served as photosensitive electrodes. Upon illumination with visible light and in the presence of $I_3^-/I^-$ as a regenerative redox couple, the OTE/$SnO_2$/[$C_{12}H_{25}$S/**5**·Au] electrode displayed a prompt generation of photocurrent. The observed photocurrents were more than two orders of magnitude greater than those obtained from previously described [60]fullerene-containing films on gold surfaces.

Porphyrins and $C_{60}$ spontaneously attract each other both in solution and in the solid state as a consequence of a set of weak forces involving π–π donor–acceptor interactions.[80,81] During the past few years, chemists have exploited this interaction to engineer supramolecular architectures in which the fullerene cage is non-covalently bound to a porphyrin.[81,82] Fukuzumi, Imahori, Kamat and co-workers have capitalised on the molecular recognition between fullerenes and porphyrins to prepare organic solar cells using porphyrin-coated gold nanoparticles intercalating $C_{60}$ molecules (Fig. 18).[83] For that purpose, several porphyrin-derived thiols, bearing linkers of different length, have been synthesised and self-assembled on gold nanoparticles ([**25*n***·Au]). Subsequently, $C_{60}$ was intercalated within SAM [**25*n***·Au] simply by immersing the porphyrin-coated nanoparticles in a toluene solution of $C_{60}$, exploiting the numerous voids present within the monolayer between neighbouring porphyrins. By mixing an equimolar solution of [**25*n***·Au] and $C_{60}$ in toluene and then injecting the mixture into a pool of $CH_3CN$ (final toluene/$CH_3CN$ 1 : 3), clusters of hybrid nanoparticles (([**25*n***·Au]·$mC_{60}$)$_z$) were formed. The clusterisation process was confirmed by dynamic light scattering analysis, which showed an increase of the average particle diameter upon raising the degree of association (from *ca.* 7 nm for [**25*n***·Au] nanoparticles in toluene to 48 and 115 nm for [**25*n***·Au] and [**25*n***·Au]·$mC_{60}$ in the 3 : 1 $CH_3CN$/toluene mixture, respectively). Such composite clusters were then deposited onto nanostructured $SnO_2$ films

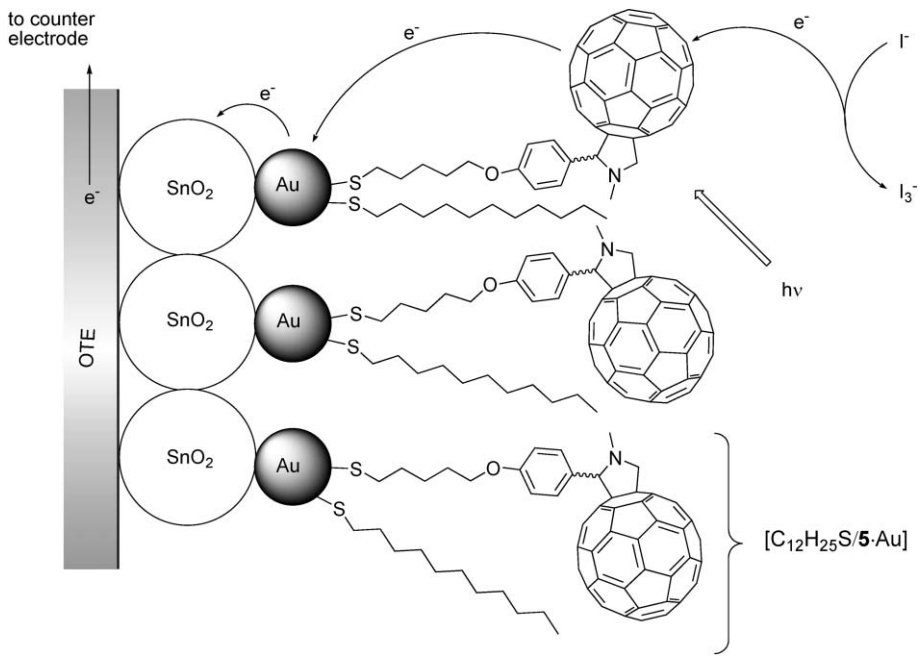


**Fig. 17** Schematic representation of the proposed mechanism of photocurrent generation at an OTE/$SnO_2$/[$C_{12}H_{25}$S/**5**·Au] electrode as reported by Thomas and co-workers.[46]

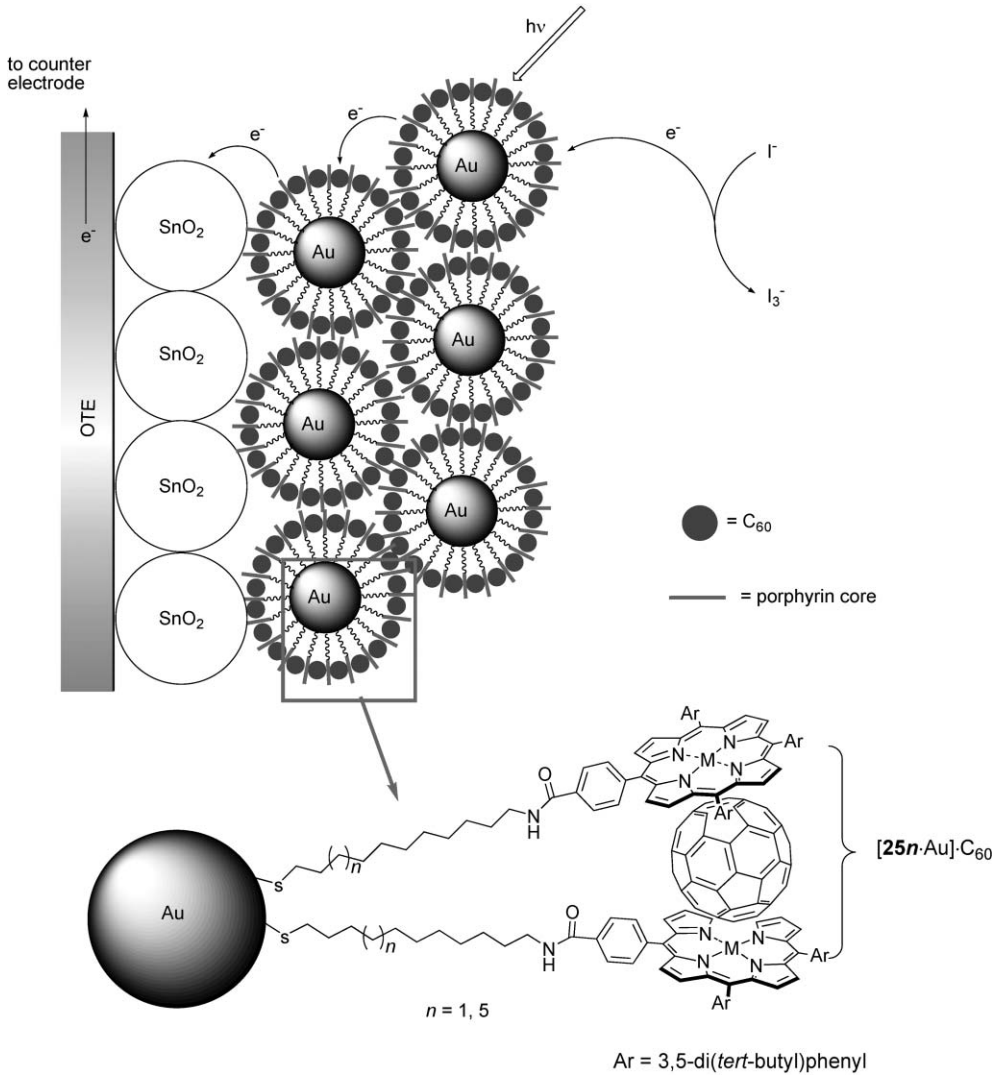


**Fig. 18** Schematic illustration of a photovoltaic cell assembled with clusters (([**25*n***·Au]·$m$C$_{60}$)$_z$) of gold nanoparticles bearing non-covalent C$_{60}$–porphyrin complexes.

*via* electrophoretic deposition to afford OTE/SnO$_2$/([**25*n***·Au]·$m$C$_{60}$)$_z$ electrodes. Upon illumination with visible light, and in the presence of $I_3^-/I^-$, the modified electrode OTE/SnO$_2$/([**25*n***·Au]·$m$C$_{60}$)$_z$ generated photocurrent, exhibiting an incident photon-to-photocurrent efficiency as high as 54% and a very broad photoactive absorption spectra reaching the NIR region (1000 nm).

### 4.1 Molecular power supplier for nanoscale machinery

One of the main challenges that is currently limiting the development of molecular machinery in real applications, is to interface an artificial molecular-based device with the macroscopic world, particularly as far as a continuous energy supply at the nanoscale level is concerned.[84,85] In fact, the first step towards the engineering of artificial molecular motors capable of exhibiting an autonomous activity (*i.e.*, to keep operating in a constant manner as long as the energy source is available) is the integration of a continuous source of electrical energy into a molecular mechanical system.[84] In this context, the groups of Stoddard and Zink first reported a photoactive energy transducer triad, consisting of conjugated TTF donor, a central porphyrin and a [60]fullerene acceptor (molecule **26** in Fig. 19) as a nanoscale power supplier to drive the de-threading of a supramolecular machinery, in the form of a donor–acceptor [2]pseudorotaxane.[86] Triad **26** self-assembled easily on Au(111) surfaces as confirmed by CV measurements ($\Gamma$(**26**) = 1.2 × $10^{-10}$ mol cm$^{-1}$). As expected, photoelectrochemical experiments carried out in a standard three-electrode cell containing SAM [**26**·Au(111)] generated a cathodic photocurrent upon irradiation with a 413 nm laser with quantum efficiencies of *ca.* 1%.

SAM [**26**·Au(111)] was then employed as molecular energy supplier for dethreading the donor–acceptor [2]pseudorotaxane [**27**·**28**]$^{4+}$ composed of a π-electron accepting cyclobis(paraquat-*p*-phenylene)cyclophane (**27**$^{4+}$) complexed with a π-electron donating 1,5-disubstituted naphthalene (**28**) (Fig. 19). In order to monitor the de-threading process, fluorescence studies were carried out. In these experiments, the enhancement of the **27**-centred emission intensity resulting

 

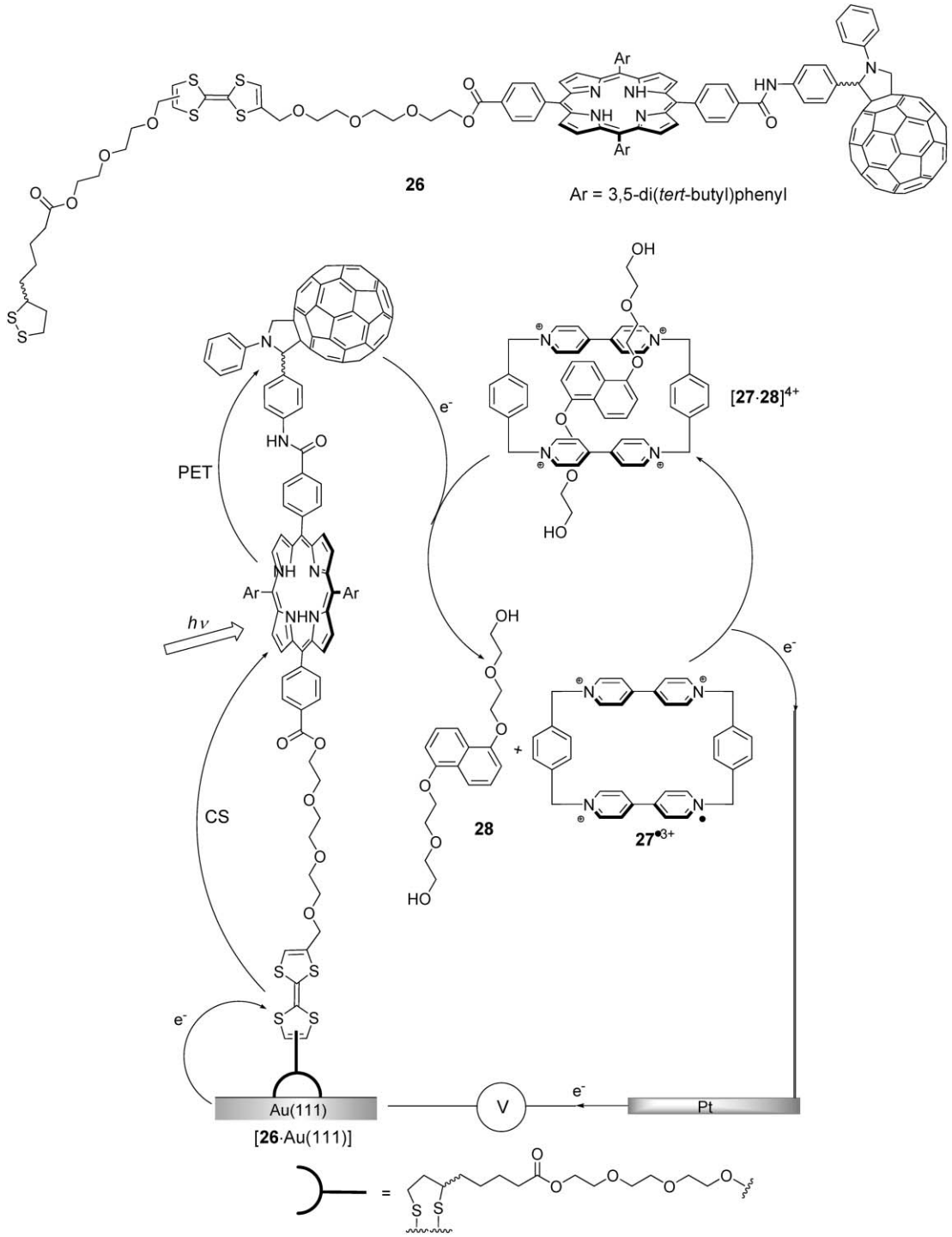


**Fig. 19** Schematic representation of the [2]pseudorotaxane dethreading mechanism as fuelled by the molecular light-driven power supplier **26**.[86]

from the dethreading of cyclophane $\mathbf{27}^{4+}$ from unit **28**, was determined. The measurements yielded a gradual increase in fluorescence emission when a working electrode coated with SAM [**26**·Au(111)] was introduced into an electrochemical cell containing a $CH_3CN$ solution of pseudorotaxane $[\mathbf{27}\cdot\mathbf{28}]^{4+}$ under irradiation conditions (413 nm) at a potential of 0 V. When the light was switched off, the **27**-centered fluorescence remained almost unaffected as a consequence of the lack of the photoinduced generation of current coming from monolayer [**26**·Au(111)]. It can be deduced that light excitation at 413 nm generated a charge separated species $TTF^{\bullet+}$–P–$C_{60}^{\bullet-}$ (*cf.* above molecule **22**) that then passed its electron from the fullerene radical anion ($E_{1/2}^{red} = -500$ mV *vs.* SCE) to the [2]pseudorotaxane [**27**·**28**] ($E_{1/2}^{red} = -300$ mV *vs.* SCE), causing the electrochemical reduction of the bis-paraquat cyclophane $\mathbf{27}^{4+}$ (to $\mathbf{27}^{\bullet 3+}$), cancelling the CT interaction and thus disassembling the [2]pseudorotaxane.

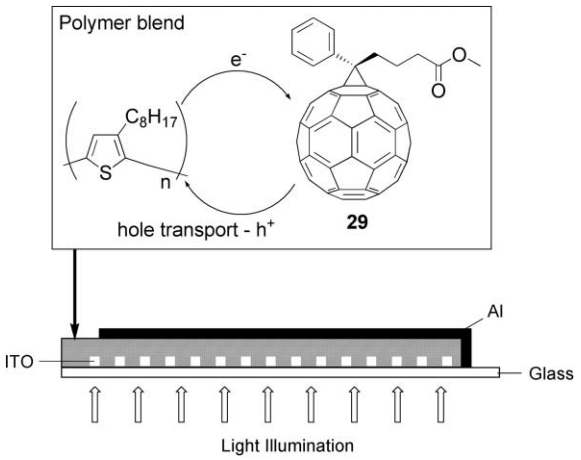


**Fig. 20** Structure of a linear photodiode array device employed as a sensor.[87]

## 5. [60]Fullerene-containing monolayer for sensing applications

In one of the few examples for the use of fullerenes in the design of sensors with real application potential, Heeger and co-workers demonstrated for the first time the feasibility of large-area image sensors made with organic photodiodes.[87] These sensors can be used as pixel elements of large-area, full-color image sensors such as linear or two-dimensional digital cameras. They consist of thin film sandwich devices with a discontinuous donor/acceptor composite. A polymer blend containing a $C_{60}$ derivative (**29**, Fig. 20) and poly(3-octylthiophene) is spin-cast onto ITO–glass substrates. Such sensors have been fabricated by simple coating of a substrate with the conjugated polymer at room temperature and at low cost. Demonstration of effective multi-band (full-color) photodetection has been shown by mounting the photodiode array on a linear translation stage which allowed an image to be focused on the surface. A document was then scanned and digitised using a personal computer with a ''multi-million color'' resolution.

In another approach, Dickert *et al.* reported the use of $C_{60}$, mixed with liquid crystals, as highly sensitive mass quartz microbalance (QMB) and surface acoustic wave (SAW) sensors for detection of diesel fuel and solvent vapors.[88] In this study, the globular character of the carbon allotrope was used rather than its physical properties. Incorporation of $C_{60}$ in liquid crystals forming nematic phases created cavities and channels in the closed-packed crystalline layer so that the organic vapor can diffuse quickly into the bulk. Thus, using a mass-sensitive device (QMB or SAW sensors) as transducer, detection of diesel fuel vapors was possible. With this amorphous layer, a resolution of 0.5% of vapor of diesel fuel in air could be attained with QMB, whereas a combination with highly sensitive SAW resonators provided a fivefold increase in sensitivity in addition to an instantaneous response.

In a collaboration with the groups of Pretsch and Echegoyen, we have reported a novel approach toward the fabrication of solid-contacted ion-selective electrodes (SC-ISEs) using SAMs [**2**·Au(111)] and [$C_8H_{17}$S/**2**·Au(111)] as intermediate layers between a valinomycin-based $K^+$-selective solvent polymeric membrane and a gold electrode (Fig. 21).[42,43] These internal contacts provided a reversible redox couple for the transduction of ionic-to-electronic conductivities and prevented the unfavorable formation of a water layer between the metal electrode and the membrane as a consequence of their high lipophilicity. All SC-ISEs based on SAMs

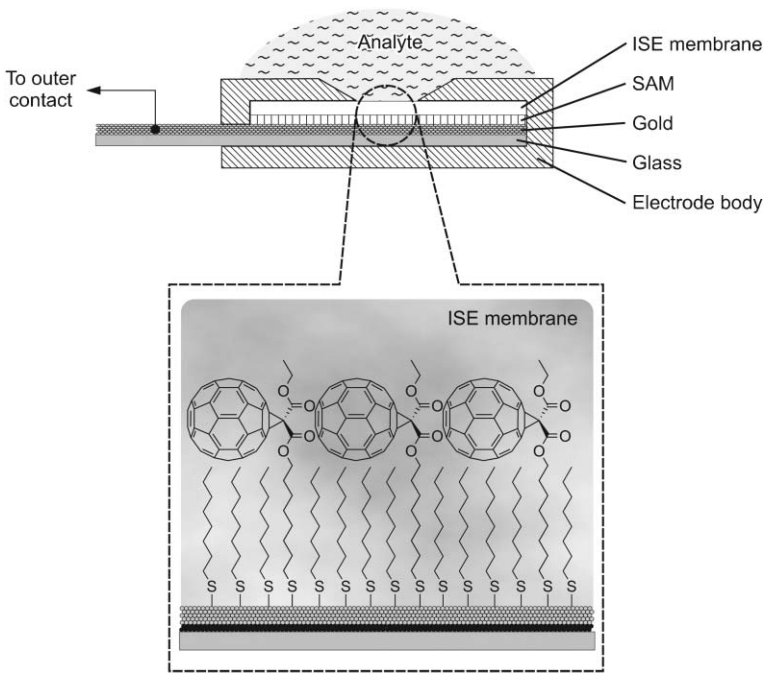


**Fig. 21** Schematic representation of the vertical cross section of a SC-ISE assembled with a mixed SAM of $C_8H_{17}SH$ and fullerene-thiol **2** ([$C_8H_{17}$S/**2**·Au(111)]).[42,43]

 

[**2**·Au(111)] and [$C_8H_{17}S$/**2**·Au(111)] were investigated for response characteristics and redox sensitivity toward $O_2$ and Fe(II)/Fe(III) solutions. As compared to a simple coated-wire configuration, SAM [**2**·Au(111)] provided improved stability and no redox and/or $O_2$ interferences as compared to classical devices lacking the fullerene-based layer. Further improvements were achieved by using SAM [$C_8H_{17}S$/**2**·Au(111)] through the acquisition of a higher lipophilicity which prevented the formation of an aqueous layer between the membrane and the metallic surface even more effectively. Therefore, these new SC-ISEs are promising for both miniaturisation and reducing the lower detection limits when compared to conventional ISEs.

## 6. [60]Fullerene-containing monolayer for biological applications

Several recent studies have shown that fullerenes exhibit interesting biological activities both *in vitro* and *in vivo*.[89] In the biological context, some elegant examples of the use of $C_{60}$ immobilised on a surface have been described. Higashi *et al.* demonstrated that positively charged SAMs on a gold substrate can immobilise double-stranded DNA without disrupting its intrinsic higher-order structure, and that site-specific cleavage of the DNA is successfully achieved by covalent incorporation of $C_{60}$ into the SAM.[90] The strategy employed in this study included the preparation, on a gold surface, of a well-ordered mixed monolayer assembly that contained (a) quaternary ammonium salts that interact electrostatically with the phosphate groups of DNA and (b) free primary amino groups for the covalent attachment of $C_{60}$ (see strategy *ii*, Fig. 1). The authors spectroscopically observed a highly guanidine-selective DNA cleavage, consistent with the involvement of singlet oxygen generated by interaction of the photoexcited fullerene core with molecular oxygen.[91]

Electrodes modified with fullerene monolayers offer exceptional electroactive interfaces capable of electronically coupling redox-active biomolecules or enzymes with electrodes and activate the respective biological function.[92] Along this line, Willner and co-workers described the use of $C_{60}$ as an electron mediator for an electrocatalysed biotransformation (Fig. 22).[93] In this work, a methano[60]fullerene carboxylic acid derivative was covalently attached to a cysteamine monolayer pre-adsorbed on a gold electrode and the resulting monolayer was shown to provide an active interface for mediating the biocatalysed oxidation of glucose to gluconic acid (Fig. 22). The fullerene moiety acts as an electron relay in the electrical communication between the electrode and a soluble glucose oxidase with an electron transfer rate constant of $k_{ET} = 3 \times 10^4\ M^{-1}\ s^{-1}$. The authors proposed that, given the size of the carbon cage, the electron mediator cannot penetrate into the protein to yield intimate contact with the FAD-site (FAD = flavin adenine dinucleotide) for electron transfer. Thus, the mediated electrical contact is assumed to proceed *via* long-distance tunneling.

With the aim of understanding the role of the co-enzyme redox couple NAD/NADH in biological redox processes involving electron transfer from a substrate, the group of Zhou and co-workers prepared a $C_{60}$–glutathione modified Au

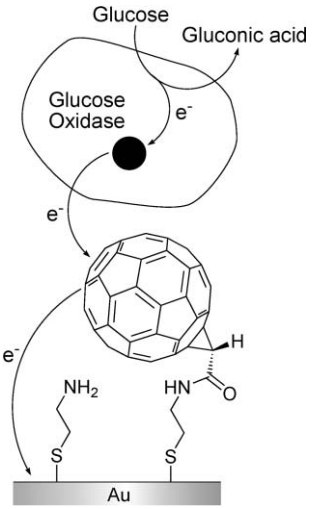


**Fig. 22** Reduction of glucose by glucose oxidase mediated by a [60]fullerene SAM covalently immobilised on Au as reported by Willner and co-workers.[93]

electrode for the electrocatalytical oxidation of NADH.[94] In this modified electrode, $C_{60}$ was covalently anchored to a pre-organised SAM of glutathione on Au. The structural properties of the fullerene-containing surface were assessed by FTIR spectroscopy, cyclic voltammetry and electrochemical impedance spectroscopy (EIS)[94]. Electrocatalysis studies (NAD/NADH oxidation processes occur at 1.10 V and 1.30 V (*vs.* SCE) at a glassy carbon and Pt electrode) revealed that the NADH form is electrochemically oxidised by the fullerene radical cation, $C_{60}^{\bullet+}$, confined on the surface. CV measurements conducted in the presence of an increasing concentration of NADH, showed a linear dependence of the current intensity with concentration, suggesting that, as more biocompatible modified electrodes become available, these fullerene-coated surfaces can represent a new class of functional materials for the detection of redox-active biological molecules.

## 7. Electronic applications of fullerene films

As shown in the previous sections, the electrochemical properties of [60]fullerene are fully maintained even when the carbon cages are confined on a surface. This behaviour allows the utilisation of $C_{60}$ as a molecular fragment for the construction of electronic devices with tunable properties such as rectifiers, data storage devices, triggers and of devices with non-linear *I*/*V*-characteristics (*i.e.*, with negative differential resistance) in which $C_{60}$ molecules act as electron-storage units or electron mediators. Thus, the incorporation of $C_{60}$ and its derivatives into well-defined networks is a very challenging goal, with a great potential for electronics applications.[95]

The first example of a [60]fullerene-containing electronic device has been reported by Joachim and Gimzewski.[96] Specifically, they constructed a molecule-based amplifier, consisting of a single $C_{60}$ molecule sandwiched between a Cu surface and a STM tip (Fig. 23). In this experiment, a signal ($V_{in}$) was applied to the piezoelectric tube that controls the *z* position of the STM tip. This induced a distortion of the $C_{60}$

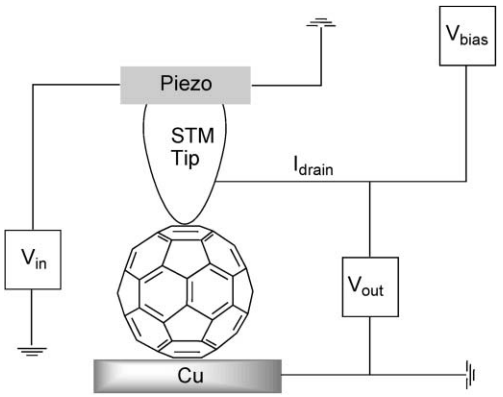


**Fig. 23** Schematic design of a single-molecule transistor based on the electromechanical interaction of an STM tip with a $C_{60}$ molecule.[96]

shape below the STM tip. Upon recording of the output signal ($V_{out}$) *vs.* the input signal ($V_{in}$), an exceptional enhancement of the conductance (two orders of magnitude) of the $C_{60}$-bridged junction was found, due to the distortion of the $C_{60}$ molecule. Such experimental evidence was supported by theoretical studies, which indicated that the HOMO and the LUMO of $C_{60}$ are shifted and broadened upon distortion, leading to an enhancement of the molecular conductive properties. The interest in $C_{60}$-based amplifiers compared to other transistor candidates arises from the fact that the amplification is effectively due to intrinsic properties of the molecule. Thus, as a second step, one can image a serial or parallel assembly of the $C_{60}$-based transistors to realise logic gates.[97]

Schönenberger and co-workers reported electron transport measurements through fullerene molecules (*i.e.*, thiol **1**) covalently immobilised within a mechanically operating Au break junction in a liquid media.[98] On changing the distance between the electrodes, *i.e.* varying the gap of the $C_{60}$-modified break junction, a peak in the conductance traces was observed, which fingerprints the presence of the fullerene molecules within the junction. The shape and intensity of such fullerene-related conductance peak revealed to be strongly influenced by the solvent surroundings (dimethyl sulfoxide or toluene), thereby showing the importance of a proper environmental control in such nanoscale junctions. The electron transport mechanism has been described invoking a resonant tunnelling model, in which the fullerene-centred LUMO level act as the resonant molecular orbital.

Another interesting approach stemming from the Aviram–Ratner model for molecular rectifiers, has been reported by Metzger and co-workers, who described a series of electrical transport measurements through a LB film of (*N*,*N*-dimethyanilino)azirino[60]fullerene **30** sandwiched between two Au electrodes (Fig. 24).[99] Asymmetric *I*/*V* characteristics were measured for all the molecularly modified devices, suggesting an unidirectional current flow between the electrodes. Such behaviour is an indication for a molecule-based rectifier, the rectification ratio (RR) of which was estimated to be $\sim$2 and $\sim$20000 at 0.6 and 1.5 V, respectively. While the system behaves as a p–n junction at low potentials (between $-1.5$ and 0.6 V), the diode shows an Ohmic characteristic at higher potential (up to 1.5 V). The perfect fitting of the *I*/*V*

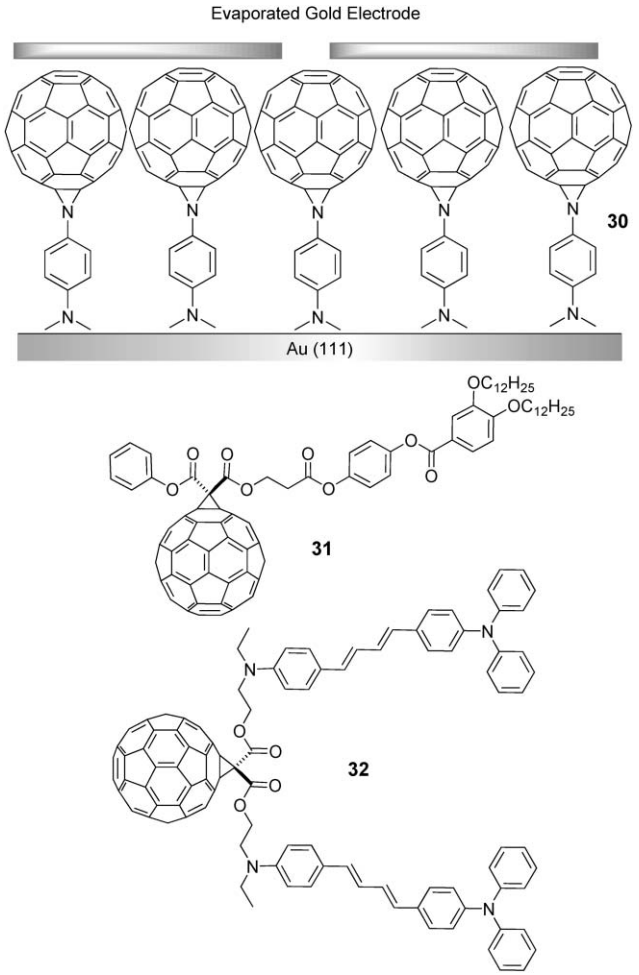


**Fig. 24** Schematic drawing of a Langmuir–Blodgett monolayer of **30** sandwiched between two gold substrates, of which the top one was gently vapor-deposited.[99] Chemical structures of other fullerene-based dyads (**31** and **32**) used as molecular rectifiers.

characteristic at low potentials (from $-1.5$ to 0.6 V) to the equation for elastic charge transport[100] confirmed the presence of a tunneling current occurring through the molecular layer. Moreover, since the *I*/*V* characteristics were very similar to those of previously reported molecular rectifiers, the same electron transport mechanism as for the Aviram–Ratner system has been invoked. In comparison to devices based on single molecules, this methodology may provide a simple alternative in the construction of [60]fullerene-based devices, owing to the easy realisation of the contact between the molecular layer and the two electrodes. LB and Langmuir–Schäfer monolayers of more complex [60]fullerene conjugates such as dyads **31**[101] and **32**[102] (Fig. 24), displayed similar rectifying behaviour as that observed for **30**, suggesting that, as more suitable technological miniaturisation methods become available, such molecules can lead to a new generation of molecule-controlled devices.

In all previously described electronic applications, the working principle of the device relies on the properties of fullerenes as single objects or as a monolayer, while the metal surface remains electronically unaltered, acting as a simple support holding the monolayer and transferring electrons.

 

Conversely, a significant perturbation of the electronic properties of the surface could be observed when various [60]fullerene-derived carboxylic acids were adsorbed on semiconductor surfaces (Fig. 25).[103] Fullerene-derived carboxylic acids **33a–d** and **34** were designed in such a way that differently sized and shaped linkers between the $C_{60}$ moiety and the surface-binding carboxyl groups would allow the investigation of the effects resulting from changes in distance and orientation between the carbon sphere and the surface. The self-assembly properties of **33a–d** and **34** were investigated on different semiconductors by means of a large variety of characterisation techniques (Fourier transform IR spectroscopy, water contact angle measurements, ellipsometry and AFM). Despite the formation of unorganised films, a strong influence of the electron-accepting fullerene cage on the superficial electronic properties of p- and n-type GaAs semiconductors, *e.g.* work function and band bending, were measured. Evidences for a fullerene-centred electron trapping on the fullerene-containing GaAs surfaces was obtained from SPV (surface photovoltage) and time-dependent CPD (contact potential difference) measurements. An opposite behaviour was detected with SAMs of carboxylic acids (especially with conjugates **33b–c**) adsorbed on ZnO surfaces. Specifically, a marked electron injection occurring from the carbon sphere to the ZnO conduction band *via* HOMO–LUMO excitation of the fullerene molecule followed by a LUMO–CB(ZnO) transition was observed. Further investigations are currently taking place in order to implant such monolayer-modified surfaces in rectifying semiconductor-based diodes.

As a part of our efforts to modify the electronic properties of inorganic surfaces, we investigated in collaboration with the Grätzel group, the cross-surface electron transfer phenomenon inside monolayers of some $C_{60}$-derived carboxylic acids (**33b**, **33d**, and **34**) anchored on nanocrystalline zirconium oxide films deposited on $SnO_2$ surfaces (see a schematic representation of the $ZrO_2$–**34** nanohybrid layer in Fig. 26).[104] These hybrid films, expected to be insulating, unexpectedly were shown to act like an electronically conducting polymer and displayed a reversible electrochemical behavior 200 times higher in intensity than that measured on a monolayer of fullerene derivative adsorbed on a flat conducting support. The strong dependence of the voltammetric response on the

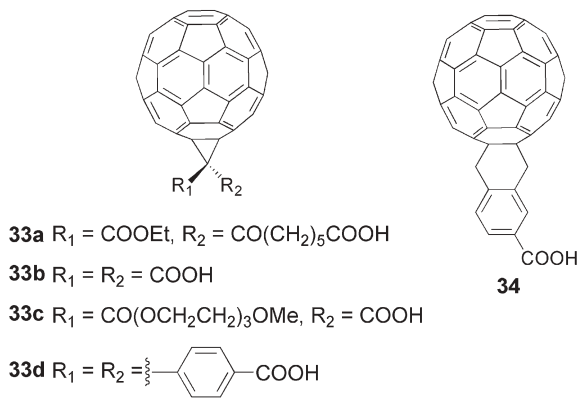


**Fig. 25** [60]Fullerene–carboxylic acid conjugates utilised to electronically tune the semiconductor and insulator surface proprieties.[103]

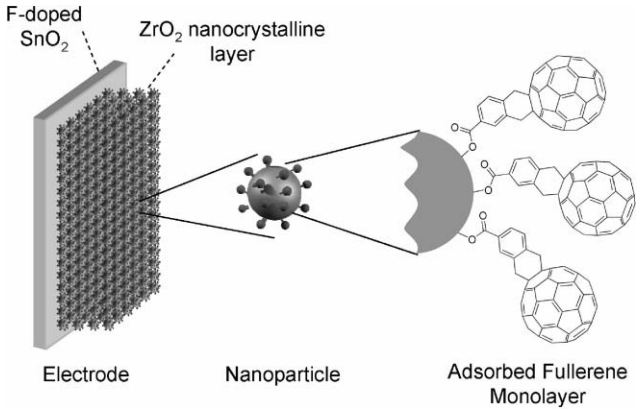


**Fig. 26** Schematic illustration of the structure of a conducting transparent oxide glass (F-doped $SnO_2$) electrode coated with $ZrO_2$ nanocrystals modified with fullerene-derived carboxylic acid **34**.[104]

concentration of the electroactive fullerene species evidenced the existence of a percolation threshold for the conductivity of the assembly which is transcended between 40 and 60% loading of the nanocrystalline film. The charge transport was found to involve a percolation/electron hopping mechanism through the entire thickness of the films. Chronocoulometry allowed the determination of apparent diffusion coefficients as high as $2 \times 10^{-8}$ $cm^2$ $s^{-1}$ for the electron hopping process. These new nanostructured films are considered to be quite promising materials since they introduce the possibility of lateral charge transport at the surface of nanocrystalline insulating layers extending their applications towards conducting inorganic–organic hybrid materials.

## 8. Conclusion

This article discusses the main strategies aimed at the preparation of ordered [60]fullerene-containing monolayers and attempts to track the evolution of their application in materials science during the last decade. The strong van der Waals interactions between the carbon spheres and the consequential tendency to form aggregates is one of the major issues in the formation of stable and structurally ordered films at the air–solid and air–water interface. Therefore, an absolutely essential requirement for the control and systematic exploration of these materials is the development of new methodologies for the incorporation of [60]fullerenes in well-defined two- and three-dimensional networks. In the first part of this review, we provided an extensive description of the four main approaches toward the production of fullerene SAMs, together with their main advantages and limitations. Specifically, we derived that direct surface modification utilising fullerene derivatives featuring suitable anchoring groups that undergo chemisorption on surface provides more stable and chemically homogeneous materials. All the photophysical (*e.g.*, singlet oxygen sensitiser) and electrochemical properties of [60]fullerenes are fully maintained even when the carbon cages are confined onto a surface.

Recent investigations hinting at potential technological applications were reviewed in the second part of this article. As extensively described with a large number of examples, a

number of fullerene-based SAMs on various surfaces have already found use as very efficient candidates for coating electrodes in photovoltaic devices. In particular, the exceptional progresses in synthetic fullerene chemistry led to the preparation of a wide variety of complex covalent and non-covalent dyads and triads modelling photoinduced electron transfer processes capable of converting light energy into electrical energy with high efficiency. Furthermore, [60]fullerene-based monolayers have been proven to be very useful scaffolds in the designing of novel high-performing sensors and biotechnological devices. Specifically, coating electrode surfaces with fullerene SAMs represents a good alternative toward the engineering of highly electroactive interfaces capable of sensing redox-active biomolecules or enzymes, and if needed, activating the respective biological function.

The incorporation of $C_{60}$ SAMs into electronic devices, although a very challenging goal, holds great expectations for engineering a new generation of molecular-based electronic devices. Specifically, the review has shown how fullerene SAMs are able to electronically tune the surface properties of some semiconductors and insulators or rectify the electron transfer behaviour occurring at the interface of a diode or junction if sandwiched between two electrodes.

Although prototypes of various functional devices have been proposed, the examples reported in this article represent only the initial steps of an increasing effort aimed at the design and preparation of further fullerene-based materials which possess all the necessary characteristics (such as structural stability under thermal and electrical stresses) for technological applications in real devices. New fullerene-based monolayer structures will continue to be developed, as more types of fullerene derivatives will be manufactured to high degrees of perfection and become commercially interesting. All this will add a new degree of sophistication of electronic and biotechnological materials based on the exceptional as well as beautiful, hollow-caged $C_{60}$ molecule.

## Acknowledgements

We gratefully acknowledge the generous financial support by the Swiss National Science Foundation, the NCCR ''Nanoscience'', the European Union (through Marie-Curie Research Training Network PRAIRIES, contract MRTN-CT-2006-035810) and MIUR (FIRB project on ''micro- and nano-structured carbon''). We are grateful to Dr Francesca Vitali for help with the artwork.

## References

1 (*a*) A. Vilan and D. Cahen, *Trends Biotechnol.*, 2002, **20**, 22; (*b*) G. Ashkenasy, D. Cahen, R. Cohen, A. Shanzer and A. Vilan, *Acc. Chem. Res.*, 2002, **35**, 121.
2 W. Krätschmer, L. D. Lamb, K. Fostiropoulos and D. R. Huffman, *Nature (London)*, 1990, **347**, 354.
3 (*a*) L. Echegoyen, F. Diederich and L. E. Echegoyen, in *Electrochemistry of Fullerenes*, ed. K. M. Kadish and R. S. Ruoff, Wiley Interscience, New York, 2000; (*b*) L. Echegoyen and L. E. Echegoyen, in *The Electrochemistry of $C_{60}$ and Related Compounds*, ed. L. Henning and O. Hammerich, Marcel Dekker, New York, 2001; (*c*) N. Armaroli, in *Photoinduced Energy Transfer Processes in Functionalized Fullerenes*, ed. D. M. Guldi and N. Martín, Kluwer Academic, Dordrecht, 2002.
4 D. M. Guldi and M. Prato, *Acc. Chem. Res.*, 2000, **33**, 695.
5 D. M. Guldi, *Chem. Commun.*, 2000, 321.
6 M. Prato and M. Maggini, *Acc. Chem. Res.*, 1998, **31**, 519.
7 (*a*) F. Diederich and R. Kessinger, *Acc. Chem. Res.*, 1999, **32**, 537; (*b*) A. Hirsch, *Top. Curr. Chem.*, 1999, **199**, 1; (*c*) S. R. Wilson, D. I. Schuster, B. Nuber, M. S. Meier, M. Maggini, M. Prato and R. Taylor, in *Organic Chemistry of Fullerenes*, ed. K. M. Kadish and R. S. Ruoff, Wiley Interscience, New York, 2000; (*d*) A. Hirsch and M. Brettreich, in *Fullerenes: Chemistry and Reactions*, Wiley-VCH, Weinheim, 2004; (*e*) A. Mateo-Alonso, D. Bonifazi and M. Prato, in *Functionalization and Applications of [60]Fullerene*, ed. L. M. Dai, Elsevier, Amsterdam, 2006.
8 D. M. Guldi and P. V. Kamat, in *Photophysical Properties of Pristine Fullerenes, Functionalized Fullerenes, and Fullerene-containing Donor-bridged Acceptor Systems*, ed. K. M. Kadish and R. S. Ruoff, Wiley Interscience, New York, 2000.
9 A. Ulman, in *An Introduction to Ultrathin Organic Films: From Langmuir-Blodgett to Self-Assembly*, San Diego, CA, 1991.
10 F. Schreiber, *Prog. Surf. Sci.*, 2000, **65**, 151.
11 For some reviews on fullerene-based Langmuir and Langmuir–Blodgett films, see: (*a*) F. Diederich and M. Gómez-López, *Chem. Soc. Rev.*, 1999, **28**, 263; (*b*) J.-F. Nierengarten, *Chem.–Eur. J.*, 2000, **6**, 3667; (*c*) J.-F. Nierengarten, *C. R. Chim.*, 2003, **6**, 725; (*d*) J.-F. Nierengarten, *New J. Chem.*, 2004, **28**, 1177; (*e*) L. Valli and D. M. Guldi, in *Langmuir Blodgett films of $C_{60}$ and $C_{60}$-Materials*, ed. D. M. Guldi and N. Martín, Kluwer Academic, Dordrecht, 2002; (*f*) A. Mateo-Alonso, C. Sooambar and M. Prato, *Org. Biomol. Chem.*, 2006, **4**, 1629; (*g*) J.-F. Nierengarten, *Top. Curr. Chem.*, 2003, **228**, 87; (*h*) D. Guillon, J.-F. Nierengarten, J.-L. Gallani, J. F. Eckert, Y. Rio, M. D. Carreon, B. Dardel and R. Deschenaux, *Macromol. Symp.*, 2003, **192**, 63.
12 D. M. Guldi and M. Prato, *Chem. Commun.*, 2004, 2517.
13 A. Ulman, *Chem. Rev.*, 1996, **96**, 1533.
14 (*a*) R. G. Nuzzo and D. L. Allara, *J. Am. Chem. Soc.*, 1983, **105**, 4481; (*b*) R. G. Nuzzo, B. R. Zegarski and L. H. Dubois, *J. Am. Chem. Soc.*, 1987, **109**, 733.
15 P. E. Laibinis, M. A. Fox, J. P. Folkers and G. M. Whitesides, *Langmuir*, 1991, **7**, 3167.
16 P. E. Laibinis and G. M. Whitesides, *J. Am. Chem. Soc.*, 1992, **114**, 9022.
17 M. E. Thompson, *Chem. Mater.*, 1994, **6**, 1168.
18 J. Sagiv, *J. Am. Chem. Soc.*, 1980, **102**, 92.
19 F. L. Dickert and A. Haunschild, *Adv. Mater.*, 1993, **5**, 887.
20 A. N. Parikh and D. L. Allara, *J. Chem. Phys.*, 1992, **96**, 927.
21 M. Zhou, J. M. Laux, K. D. Edwards, J. C. Hemminger and B. Hong, *Chem. Commun.*, 1997, 1977.
22 K. Mathauer and C. W. Frank, *Langmuir*, 1993, **9**, 3002.
23 R. M. A. Azzam and N. M. Bashara, *Ellipsometry and Polarized Light*, North-Holland, Amsterdam, 1987.
24 K. A. Peterlinz and R. Georgiadis, *Langmuir*, 1996, **12**, 4731.
25 J. C. Vickerman, in *Surface Analysis, the Principal Techniques*, Wiley, Chichester, 1997.
26 T. D. McCarley and R. L. McCarley, *Anal. Chem.*, 1997, **69**, 130.
27 (*a*) A. A. Gewirth and B. K. Niece, *Chem. Rev.*, 1997, **97**, 1129; (*b*) S. N. Maganov and M.-H. Whangbo, *Surface Analysis with STM and AFM, Experimental and Theoretical Aspects of Image Analysis*, VCH, Weinheim, 1996.
28 H. O. Finklea, in *Electrochemistry of Organized Monolayers of Thiols and Related Molecules on Electrodes*, ed. A. J. Bard and I. Rubinstein, Marcel Dekker, New York, 1996.
29 M. J. Rosseinsky, *Chem. Mater.*, 1998, **10**, 2665.
30 R. Wilson, G. Meijer, D. Bethune, R. Johnson, D. Chambliss, M. de Vries, H. Hunziker and H. Wendt, *Nature (London)*, 1990, **348**, 621.
31 A. V. Hamza, in *Fullerene-Surface Interactions*, ed. K. M. Kadish and R. S. Ruoff, Wiley Interscience, New York, 2000.
32 E. I. Altman and R. J. Colton, *Surf. Sci.*, 1993, **295**, 13.
33 K. Tanigaki, S. Kuroshima and T. W. Ebbesen, *Thin Solid Films*, 1995, **257**, 154.
34 R. Signorini, R. Bozio and M. Prato, in *Opical Limiting Applications*, ed. D. M. Guldi and N. Martín, Kluwer Academic, Dordrecht, 2002.
35 G. Brusatin and R. Signorini, *J. Mater. Chem.*, 2002, **12**, 1964.
36 X. Shi, W. B. Caldwell, K. Chen and C. A. Mirkin, *J. Am. Chem. Soc.*, 1994, **116**, 11598.

 

37 C. Pan, M. P. Sampson, Y. Chai, R. H. Hauge and J. L. Margrave, *J. Phys. Chem.*, 1991, **95**, 2944.
38 R. G. Nuzzo, L. H. Dubois and D. L. Allara, *J. Am. Chem. Soc.*, 1990, **112**, 558.
39 (*a*) P. Dietz, P. K. Hansma, K. Fostiropoulos and W. Krätschmer, *Appl. Phys. A: Mater. Sci. Process.*, 1993, **56**, 207; (*b*) P. Dietz, K. Fostiropoulos, W. Krätschmer and P. K. Hansma, *Appl. Phys. Lett.*, 1992, **60**, 62.
40 F. Y. Song, S. Zhang, D. Bonifazi, O. Enger, F. Diederich and L. Echegoyen, *Langmuir*, 2005, **21**, 9246.
41 O. Enger, F. Nuesch, M. Fibbioli, L. Echegoyen, E. Pretsch and F. Diederich, *J. Mater. Chem.*, 2000, **10**, 2231.
42 M. Fibbioli, K. Bandyopadhyay, S.-G. Liu, L. Echegoyen, O. Enger, F. Diederich, D. Gingery, P. Bühlmann, H. Persson, U. W. Suter and E. Pretsch, *Chem. Mater.*, 2002, **14**, 1721.
43 M. Fibbioli, K. Bandyopadhyay, S.-G. Liu, L. Echegoyen, O. Enger, F. Diederich, E. Pretsch and P. Bühlmann, *Chem. Commun.*, 2000, 2231.
44 T. Gu, J. K. Whitesell and M. A. Fox, *J. Org. Chem.*, 2004, **69**, 4075.
45 S. H. Kang, H. Ma, M. S. Kang, K. S. Kim, A. K. Y. Jen, M. H. Zareie and M. Sarikaya, *Angew. Chem., Int. Ed.*, 2004, **43**, 1512.
46 P. K. Sudeep, B. I. Ipe, K. G. Thomas, M. V. George, S. Barazzouk, S. Hotchandani and P. V. Kamat, *Nano Lett.*, 2002, **2**, 29.
47 Y. S. Shon, K. F. Kelly, N. J. Halas and T. R. Lee, *Langmuir*, 1999, **15**, 5329.
48 V. T. Hoang, L. M. Rogers and F. D'Souza, *Electrochem. Commun.*, 2002, **4**, 50.
49 K. S. Kim, M. S. Kang, H. Ma and A. K. Y. Jen, *Chem. Mater.*, 2004, **16**, 5058.
50 S.-G. Liu, C. Martineau, J.-M. Raimundo, J. Roncali and L. Echegoyen, *Chem. Commun.*, 2001, 913.
51 O. Dominguez, L. Echegoyen, F. Cunha and N. J. Tao, *Langmuir*, 1998, **14**, 821.
52 (*a*) C. Du, B. Xu, Y. Li, C. Wang, S. Wang, Z. Shi, H. Fang, S. Xiao and D. Zhu, *Langmuir*, 2001, **17**, 1191; (*b*) C. Du, B. Xu, Y. Li, C. Wang, S. Wang, Z. Shi, H. Fang, S. Xiao and D. Zhu, *New J. Chem.*, 2001, **25**, 1191.
53 K. M. Chen, W. B. Caldwell and C. A. Mirkin, *J. Am. Chem. Soc.*, 1993, **115**, 1193.
54 W. B. Caldwell, K. Chen, C. A. Mirkin and S. J. Babinec, *Langmuir*, 1993, **9**, 1945.
55 V. V. Tsukruk, L. M. Lander and W. J. Brittain, *Langmuir*, 1994, **10**, 996.
56 L. M. Lander, W. J. Brittain and V. Tsukruk, *Polym. Prepr. (Am. Chem. Soc., Div. Polym. Chem.)*, 1994, **35**, 488.
57 F. Arias, L. A. Godinez, S. R. Wilson, A. E. Kaifer and L. Echegoyen, *J. Am. Chem. Soc.*, 1996, **118**, 6086.
58 C. Luo, D. M. Guldi, M. Maggini, E. Menna, S. Mondini, N. A. Kotov and M. Prato, *Angew. Chem., Int. Ed.*, 2000, **39**, 3905.
59 D. M. Guldi, F. Pellarini, M. Prato, C. Granito and L. Troisi, *Nano Lett.*, 2002, **2**, 965.
60 A. Gulino, S. Bazzano, G. G. Condorelli, S. Giuffrida, P. Mineo, C. Satriano, E. Scamporrino, G. Ventimiglia, D. Vitalini and I. Fragalà, *Chem. Mater.*, 2005, **17**, 1079.
61 T. Hatano, A. Ikeda, T. Akiyama, S. Yamada, M. Sano, Y. Kanekiyo and S. Shinkai, *J. Chem. Soc., Perkin Trans. 2*, 2000, **5**, 909.
62 A. Ikeda, T. Hatano, S. Shinkai, T. Akiyama and S. Yamada, *J. Am. Chem. Soc.*, 2001, **123**, 4855.
63 S. Zhang, A. Palkar, A. Fragoso, P. Prados, J. de Mendoza and L. Echegoyen, *Chem. Mater.*, 2005, **17**, 2063.
64 S. Zhang and L. Echegoyen, *C. R. Chim.*, 2006, **9**, 1031.
65 S. Zhang and L. Echegoyen, *Tetrahedron*, 2006, **62**, 1947.
66 (*a*) J. A. Theobald, N. S. Oxtoby, M. A. Phillips, N. R. Champness and P. H. Beton, *Nature (London)*, 2003, **424**, 1029; (*b*) J. A. Theobald, P. H. Beton, N. S. Oxtoby, N. R. Champness and T. J. S. Dennis, *Langmuir*, 2005, **21**, 2038.
67 H. Spillmann, A. Kiebele, M. Stöhr, T. Jung, D. Bonifazi, F. Cheng and F. Diederich, *Adv. Mater.*, 2006, **18**, 275.
68 D. Bonifazi, H. Spillmann, A. Kiebele, M. de Wild, P. Seiler, F. Y. Cheng, H. J. Guntherodt, T. Jung and F. Diederich, *Angew. Chem., Int. Ed.*, 2004, **43**, 4759.
69 A. Kiebele, D. Bonifazi, F. Cheng, M. Stöhr, F. Diederich, T. Jung and H. Spillmann, *ChemPhysChem*, 2006, **7**, 1462.
70 H. Imahori and Y. Sakata, *Eur. J. Org. Chem.*, 1999, 2445.
71 For some recent reviews on fullerene-dyads see: (*a*) D. M. Guldi, G. M. A. Rahman, V. Sgobba and C. Ehli, *Chem. Soc. Rev.*, 2006, **35**, 471; (*b*) D. M. Guldi, *Chem. Soc. Rev.*, 2002, **31**, 22; (*c*) H. Imahori, Y. Mori and Y. Matano, *J. Photochem. Photobiol., C*, 2003, **4**, 51; (*d*) N. Armaroli, *Photochem. Photobiol. Sci.*, 2003, **2**, 73; (*e*) J. L. Segura, N. Martín and D. M. Guldi, *Chem. Soc. Rev.*, 2005, **34**, 31; (*f*) L. Sánchez, M. A. Herranz and N. Martín, *J. Mater. Chem.*, 2005, **15**, 1409; (*g*) L. Sánchez, N. Martín and D. M. Guldi, *Angew. Chem., Int. Ed.*, 2005, **44**, 5374. For some very recent developments: (*h*) D. Bonifazi, M. Scholl, F. Y. Song, L. Echegoyen, G. Accorsi, N. Armaroli and F. Diederich, *Angew. Chem., Int. Ed.*, 2003, **42**, 4966; (*i*) F. Langa, M. J. Gomez-Escalonilla, J. M. Rueff, T. M. F. Duarte, J.-F. Nierengarten, V. Palermo, P. Samori, Y. Rio, G. Accorsi and N. Armaroli, *Chem.–Eur. J.*, 2005, **11**, 4405; (*j*) D. Bonifazi, G. Accorsi, N. Armaroli, F. Song, A. Palkar, L. Echegoyen, M. Scholl, P. Seiler, B. Jaun and F. Diederich, *Helv. Chim. Acta*, 2005, **88**, 1839; (*k*) T. Konishi, A. Ikeda and S. Shinkai, *Tetrahedron*, 2005, **61**, 4881; (*l*) F. Cardinali, H. Mamlouk, Y. Rio, N. Armaroli and J.-F. Nierengarten, *Chem. Commun.*, 2004, 1582; (*m*) T. M. Figueira-Duarte, J. Clifford, V. Amendola, A. Gegout, J. Olivier, F. Cardinal, M. Meneghetti, N. Armaroli and J.-F. Nierengarten, *Chem. Commun.*, 2006, 2054; (*n*) F. Marotti, D. Bonifazi, R. Gehrig, J. L. Gallani and F. Diederich, *Isr. J. Chem.*, 2005, **45**, 303; (*o*) S. Campidelli, E. Vazquez, D. Milic, M. Prato, J. Barbera, D. M. Guldi, M. Marcaccio, D. Paolucci, F. Paolucci and R. Deschenaux, *J. Mater. Chem.*, 2004, **14**, 1266; (*p*) L. Sánchez, M. Sierra, N. Martín, A. J. Myles, T. J. Dale, J. Rebek, W. Seitz and D. M. Guldi, *Angew. Chem., Int. Ed.*, 2006, **45**, 4637; (*q*) W. S. Li, K. S. Kim, D. L. Jiang, H. Tanaka, T. Kawai, J. H. Kwon, D. Kim and T. Aida, *J. Am. Chem. Soc.*, 2006, **128**, 10527; (*r*) A. Mateo-Alonso, C. Sooambar and M. Prato, *C. R. Chim.*, 2006, **9**, 44.
72 D. Gust, T. A. Moore and A. L. Moore, *Acc. Chem. Res.*, 2001, **34**, 40.
73 H. Imahori, N. V. Tkachenko, V. Vehmanen, K. Tamaki, H. Lemmetyinen, Y. Sakata and S. Fukuzumi, *J. Phys. Chem. A*, 2001, **105**, 1750.
74 T. Akiyama, H. Imahori, A. Ajawakom and Y. Sakata, *Chem. Lett.*, 1996, 907.
75 (*a*) H. Imahori, T. Azuma, A. Ajavakom, H. Norieda, H. Yamada and Y. Sakata, *J. Phys. Chem. B*, 1999, **103**, 7233; (*b*) H. Imahori, T. Azuma, S. Ozawa, H. Yamada, K. Ushida, A. Ajavakom, H. Norieda and Y. Sakata, *Chem. Commun.*, 1999, 557.
76 H. Imahori, H. Yamada, S. Ozawa, K. Ushida and Y. Sakata, *Chem. Commun.*, 1999, 1165.
77 (*a*) H. Imahori and S. Fukuzumi, *Adv. Funct. Mater.*, 2004, **14**, 525; (*b*) H. Imahori, K. Hosomizu, M. Kimura, S. Fukuzumi, T. Sato, Y. Nishimura, K. A. Tae, D. Kim, K. K. Seong, I. Yamazaki, Y. Araki and O. Ito, *Chem.–Eur. J.*, 2004, **10**, 5111; (*c*) H. Imahori, Y. Kashiwagi, T. Hasobe, M. Kimura, S. Fukuzumi, T. Hanada, Y. Nishimura, I. Yamazaki, Y. Araki and O. Ito, *Thin Solid Films*, 2004, **451**, 580.
78 D. Hirayama, K. Takimiya, Y. Aso, T. Otsubo, T. Hasobe, H. Yamada, H. Imahori, S. Fukuzumi and Y. Sakata, *J. Am. Chem. Soc.*, 2002, **124**, 532.
79 Y. J. Cho, T. K. Ahn, H. Song, K. S. Kim, C. Y. Lee, W. S. Seo, K. Lee, S. K. Kim, D. Kim and J. T. Park, *J. Am. Chem. Soc.*, 2005, **127**, 2380.
80 Y.-B. Wang and Z. Lin, *J. Am. Chem. Soc.*, 2003, **125**, 6072.
81 P. D. W. Boyd and C. A. Reed, *Acc. Chem. Res.*, 2005, **38**, 235.
82 (*a*) P. D. W. Boyd, M. C. Hodgson, C. E. F. Rickard, A. G. Oliver, L. Chaker, P. J. Brothers, R. D. Bolskar, F. S. Tham and C. A. Reed, *J. Am. Chem. Soc.*, 1999, **121**, 10487; (*b*) J.-Y. Zheng, K. Tashiro, Y. Hirabayashi, K. Kinbara, K. Saigo, T. Aida, S. Sakamoto and K. Yamaguchi, *Angew. Chem., Int. Ed.*, 2001, **40**, 1858; (*c*) M. Ayabe, A. Ikeda, Y. Kubo, M. Takeuchi and S. Shinkai, *Angew. Chem., Int. Ed.*, 2002, **41**, 2790; (*d*) D. Sun, F. S. Tham, C. A. Reed and P. D. W. Boyd, *Proc. Natl. Acad. Sci. U. S. A.*, 2002, **99**, 5088.
83 (*a*) T. Hasobe, H. Imahori, P. V. Kamat, T. K. Ahn, S. K. Kim, D. Kim, A. Fujimoto, T. Hirakawa and S. Fukuzumi, *J. Am.*

*Chem. Soc.*, 2005, **127**, 1216; (*b*) T. Hasobe, H. Imahori, P. V. Kamat and S. Fukuzumi, *J. Am. Chem. Soc.*, 2003, **125**, 14962.
84 (*a*) V. Balzani, A. Credi, B. Ferrer, S. Silvi and M. Venturi, *Top. Curr. Chem.*, 2005, **262**, 1; (*b*) V. Balzani, A. Credi, F. M. Raymo and J. F. Stoddart, *Angew. Chem., Int. Ed.*, 2000, **39**, 3349.
85 A. Credi, *Aust. J. Chem.*, 2006, **59**, 157.
86 S. Saha, E. Johansson, A. H. Flood, H. R. Tseng, J. I. Zink and J. F. Stoddart, *Chem.–Eur. J.*, 2005, **11**, 6846.
87 G. Yu, J. Wang, J. McElvain and A. J. Heeger, *Adv. Mater.*, 1998, **10**, 1431.
88 F. L. Dickert, M. E. Zenkel, W.-E. Bulst, G. Fischerauer and U. Knauer, *Fresenius' J. Anal. Chem.*, 1996, **357**, 27.
89 (*a*) S. Bosi, T. Da Ros, G. Spalluto and M. Prato, *Eur. J. Org. Chem.*, 2001, 913; (*b*) E. Nakamura and H. Isobe, *Acc. Chem. Res.*, 2003, **36**, 807.
90 N. Higashi, T. Inoue and M. Niwa, *Chem. Commun.*, 1997, 1507.
91 R. Bernstein, F. Prat and C. S. Foote, *J. Am. Chem. Soc.*, 1999, **121**, 464.
92 For a recent review on fullerene-based sensors for biological applications see: B. S. Sherigara, W. Kutner and F. D'Souza, *Electroanalysis (N. Y.)*, 2003, **15**, 753.
93 F. Patolsky, G. L. Tao, E. Katz and I. Willner, *J. Electroanal. Chem.*, 1998, **454**, 9.
94 F. Cheng and X. Zhou, *Electroanalysis (N. Y.)*, 2001, **13**, 949.
95 R. L. Carroll and C. B. Gorman, *Angew. Chem., Int. Ed.*, 2002, **41**, 4378.
96 (*a*) C. Joachim and J. K. Gimzewski, *Chem. Phys. Lett.*, 1997, **265**, 353; (*b*) C. Joachim, J. K. Gimzewski and H. Tang, *Phys. Rev. B*, 1998, **58**, 116407.
97 C. Joachim, J. K. Gimzewski and A. Aviram, *Nature (London)*, 2000, **408**, 541.
98 L. Grüter, F. Cheng, T. Theikkilä, M. T. González, F. Diederich, C. Schönenberger and M. Calame, *Nanotechnology*, 2005, **16**, 2143.
99 R. M. Metzger, J. W. Baldwin, W. J. Shumate, I. R. Peterson, P. Mani, G. J. Mankey, T. Morris, G. Szulczewski, S. Bosi, M. Prato, A. Comito and Y. Rubin, *J. Phys. Chem. B*, 2003, **107**, 1021.
100 I. R. Petersen, D. Vuillaume and R. M. Metzger, *J. Phys. Chem. A*, 2001, **105**, 4702.
101 S. S. Gayathri and A. Patnaik, *Chem. Commun.*, 2006, 1977.
102 A. Honciuc, A. Jaiswal, A. Gong, H. Ashworth, C. W. Spangler, I. R. Peterson, L. R. Dalton and R. M. Metzger, *J. Phys. Chem. B*, 2005, **109**, 857.
103 D. Bonifazi, A. Salomon, O. Enger, F. Diederich and D. Cahen, *Adv. Mater.*, 2002, **14**, 802.
104 N. Papageorgiou, M. Grätzel, O. Enger, D. Bonifazi and F. Diederich, *J. Phys. Chem. B*, 2002, **106**, 3813.

 